Supporting Information

Copper doping boosts catalase-like activity of atomically precise gold nanoclusters for cascade reactions combined with urate oxidase in ZIF-8 matrix

Yi-Shu Wang,‡ Yan Chen,‡ Chen Dong, Zhao-Yang Wang, Jinmeng Cai, Xueli Zhao, Hui-Lin Mo* and Shuang-Quan Zang*

Tianjian Laboratory of Advanced Biomedical Sciences, Institute of Advanced Biomedical Sciences, Henan Key Laboratory of Crystalline Molecular Functional Materials, Henan International Joint Laboratory of Tumor Theranostic Cluster Materials, Green Catalysis Center and College of Chemistry, Zhengzhou University, Zhengzhou 450001, China

*Corresponding authors (E-mail: zangsqzg@zzu.edu.cn, mohl@zzu.edu.cn)

[‡] These authors contributed equally to this work

Table of Contents

1. Experimental Section

Reagents and Chemicals.

All reagents and solvents used were of commercially available reagent grade and used without further purification. Gold chloride ($HAuCl_4 \cdot 3H_2O$) was purchased from Alfa Aesar. MPA was obtained from TCI. Copper nitrate ($Cu(NO_3)_2$), zinc nitrate ($Zn(NO_3)_2$), and 2-Methylimidazole were purchased from Aladdin. Sodium hydroxide (NaOH) was purchased from Yong Da Chemical. The Catalase Assay Kit and BCA protein assay kit were purchased from Beyotime Biotechnology. HRP and fluorescein isothiocyanate (FITC) were obtained from Sangon Biotech. Uricase, trypsin and 3,3',5,5'-Tetramethylbenzidine (TMB) were purchased from Solarbio. Uric acid was obtained from Energy Chemical.

Characterization.

Ultraviolet-visible (UV-vis) spectroscopy was recorded on a PerkinElmer EnSight HH3400 spectrophotometer. Bruker microTOF-Q system was employed to obtain Electrospray ionization mass spectra (ESI-MS). Inductively coupled plasma mass spectrometry (ICP-MS) was performed on a X Series ICP-MS (Thermo Fisher Scientific). X-ray photoelectron spectroscopy (XPS) measurements were taken by a ESCALAB 250Xi spectrometer. Fourier transform infrared (FTIR) spectra were measured on Nicolet NEXUS 470-FTIR. Raman spectra were collected at room temperature using a 532 nm single-frequency diode laser (Spectra-Physics) with and a CCD detector (LabRAm HR Evolution). ζ potential were measured by Horiba Scientific Nanopartica Nano Particle Analyzer SZ-100V2. Transmission electron microscopy (TEM) images and EDS mapping of elemental distributions were measured on a FEI TECNAIG2F20-S-TWIN high-resolution transmission electron microscope operating. Powder X-ray diffraction (PXRD) patterns were recorded using X'Pert PRO diffractometer with a Cu Kα anode (λ= 1.54178 Å) at 40 kV and 20 mA. Confocal laser scanning microscopy (CLSM) images were collected by using Leica TCS SP8 X confocal microscope.

Synthesis of $Au_{25}(MPA)_{18}$ and $Au_{24}M_1(MPA)_{18}$

Synthesis of $Au_{25}(MPA)_{18}$ was referred to the previously reported literature with moderate modifications.[1,2] Briefly, $HAuCl_4$ aqueous solutions (40 mM, 0.25 mL) and MPA (100 mM, 0.2 mL) were added to water (4.55 mL) and stirred at room temperature for 5 min. Then the pH of the mixed solution was adjusted to 12.0 by dropwise adding aqueous solution of 5 mM NaOH. After 30 min, The CO was introduced into the solution for 5 min. The reaction vessel was then kept airtight and the reaction was allowed to proceed for 24 h under gentle stirring (500 rpm) at room temperature. For further purification of nanoclusters, A 3 kDa ultrafiltration tube at 3500 rpm/min was used to remove smaller organic ligands. The obtained samples are stored in dark at 4 °C for further analysis. Synthesis of $Au_{24}M_1MPA_{18}$ (M=Cu or Zn) was following the same method by replacing the Au atoms in $HAuCl_4$ (40 mM, 0.25 mL) with various nitrate metal ions (Cu^{2+}, Zn^{2+}) at a 4% molar ratio (Au : M = 24:1).[3,4]

Preparation of UOx@ZIF-8 and UOx-$Au_{24}Cu_1$@ZIF-8

In detail, 1 mL of 2-methylimidazole (0.7 M) containing 600 μg of $Au_{24}Cu_1$ and 300 μg of UOx was stirred gently at room temperature. Afterward, 1 mL of zinc nitrate hexahydrate (10 mM) was added quickly, and the mixture was stirred overnight at room temperature. Then the final product was centrifuged (8000 rpm, 5 min) and washed with ultrapure water three times.Synthesis of UOx@ZIF-8 composite was following the same protocol by replacing the multi-enzyme solution with UOx (UOx in UOx@ZIF-8 amount is equal to that of UOx in UOx-$Au_{24}Cu_1$@ZIF-8).

Synthesis of FITC-UOx@ZIF-8 and FITC-UOx-$Au_{24}Cu_1$@ZIF-8

FITC saturated aqueous solution (200 μL) was added to UOx solution (200 μL, 5 mg/mL), followed by shaking at room temperature in the dark. Dialysis bag (3500 D) was used to remove free FITC. FITC-UOx was collected after 48 h. Synthesis of FITC-UOx@ZIF-8 or FITC-UOx-$Au_{24}Cu_1$@ZIF-8 was following the same method of UOx@ZIF-8 and UOx-$Au_{24}Cu_1$@ZIF-8.

Loading amount

The enzyme concentration was analyzed according to the standard protocol of the BCA protein assay kit. The UOx loading efficacy (%) was calculated using Eq. 1:

$$\text{UOx loading efficacy (\%)}=\frac{m_0\text{-}m_1}{m}\times 100$$

where m_0 (mg), m_1 (mg) and m (mg) represent the weight of UOx before encapsulation, UOx of the supernatants after immobilization and ZIF-8, respectively.

The loading content of UOx in ZIF-8 determined by BCA assay using UV–vis spectroscopy was about 30%, resulting from the decreased characteristic peak absorption value in the supernatant before and after encapsulation process.

X-ray absorption spectroscopy measurements and data processing.

Au-L_3 edge and Cu K-edge were obtained with Si (111) crystal monochromators at the BL11B beamlines at the Shanghai Synchrotron Radiation Facility (SSRF) (Shanghai, China). Before the analysis at the beamline, samples were pressed into thin sheets with 1 cm in diameter and sealed using Kapton tape film. The XAFS spectra were recorded at room temperature using a 4-channel Silicon Drift Detector (SDD) Bruker 5040. Au-L_3 edge extended X-ray absorption fine structure (EXAFS) spectra of Au_{25} was recorded in transmission mode. Au-L_3 edge and Cu K-edge extended X-ray absorption fine structure (EXAFS) spectra of $Au_{24}Cu_1$ and UOx-$Au_{24}Cu_1$@ZIF-8 were obtained in fluorescence mode. Negligible changes in the line-shape and peak position of Au-L_3 edge and Cu K-edge XANES spectra were observed between two scans taken for a specific sample.

Data reduction, data analysis, and EXAFS fitting were performed and analyzed with the Athena and Artemis programs of the Demeter data analysis packages that utilizes the FEFF6 program to fit the EXAFS data. The energy calibration of the sample was conducted through standard and Au foil and Cu foil, which as a reference was simultaneously measured. A linear function was subtracted from the pre-edge region, then the edge jump was normalized using Athena software. The $\chi(k)$ data were isolated by subtracting a smooth, third-order polynomial approximating the absorption background of an isolated atom. The k3-weighted χ(k) data were Fourier transformed after applying a HanFeng window function (Δk = 1.0). For EXAFS modeling, The global amplitude EXAFS (CN, R, σ2 and ΔE0) were obtained by nonlinear fitting, with least-squares refinement, of the EXAFS equation to the Fourier-transformed data in R-space, using Artemis software, EXAFS of the Au foil and Cu foil are fitted and the obtained amplitude reduction factor S02 value (0.839 and 0.890) was set in the EXAFS analysis to determine the coordination numbers (CNs) in the Au-S and Cu-S scattering path in sample.

Computational details

The density functional theory (DFT)[5] calculations were performed by using the Gaussian 16 program. The geometric structures of all involved transition states were optimized by using the M06-2X density functional, combined with the def2-SVP. The harmonic frequency calculations were conducted at the same level to corroborate each transition state has one and only one imaginary frequency and other structures have no imaginary frequency. The 3D structures of the molecules were rendered by using the CYLview.[6]

$$M + H_2O_2 \rightleftarrows M - OH + OH \quad eq2$$
$$OH + H_2O_2 \rightarrow H_3O_3 \rightarrow H_2O + HO_2 \quad eq3$$
$$M - OH + HO_2 \rightarrow M + H_2O + O_2 \quad eq4$$

CAT-like properties test

The activities of catalase (CAT) were measured using Catalase Assay Kit. H_2O_2 (250 mM, 10 μL) and Au NCs (10 mg/mL, 12 μL) were added to the centrifuge tube and incubation for 5 min at 25 °C. The remaining H_2O_2 can oxidize the chromogenic substrate under the catalysis of peroxide to produce a red product (N-4-antipyryl-3-chloro-5-sulfonate-p-benzoquinonemonoimine), which can be detected in a 96-well plate at 520 nm. CAT activity was measured by measuring the decomposition of H_2O_2 using a UV-Visible spectrophotometer.

The reaction solutions contained 3 mg/mL of Au NCs and 5 mM H_2O_2 in deionized water for different time (0-20 h) to obtain the photos of O_2 production.

Kinetic assessment of the CAT-like activity of AuNCs was measured by monitoring the increase in O_2 concentration with an oxygen probe (JPBJ-608 Portable Dissolved Oxygen Meter). Different concentrations of H_2O_2 (50–300 mM) and 0.5 mg/ml of AuNCs were added to the system to monitor the solubility change of O_2 every 5 s at pH 7.0 at room temperature.

The initial reaction rates were calculated from the slope of O_2 generation and applied to the Michaelis–Menten equation as Eq. 5:

$$v = \frac{v_{max}[S]}{K_m + [S]}$$

where v is the mean velocity, v_{max} is the maximal reaction velocity, [S] is the initial concentration of the substrate, and K_m is the Michaelis−Menten constant.

The values of the kinetic parameters (v_{max} and K_m) were calculated by the Lineweaver-Burk Plot as Eq. 6:

$$\frac{1}{v} = \frac{K_m}{v_{max}} \times \frac{1}{[S]} + \frac{1}{v_{max}}$$

After detection the velocity versus vary concentration of substrate, a plot of l/[S] against 1/v according to the Eq. 6 gave a straight line. The V_{max} and K_m could be acquired by the slope and intercept of this line.

Effect of pH, Time, and Temperature on the Activity of Au NCs

Effect of pH: Au NCs (2.4 mg/mL Au_{25}, $Au_{24}Cu_1$ or $Au_{24}Zn_1$) were incubated with H_2O_2 (250 mM, 10 μL) in different PBS buffer (pH 4.0 to 8.0) at 25 °C for 5 min.

Effect of time: Au NCs (2.4 mg/mL Au_{25}, $Au_{24}Cu_1$ or $Au_{24}Zn_1$) were incubated with H_2O_2 (250 mM, 10 μL) at 25 °C for different time (5-300 min).

Effect of temperature: Au NCs (2.4 mg/mL Au_{25}, $Au_{24}Cu_1$ or $Au_{24}Zn_1$) were incubated with H_2O_2 (250 mM, 10 μL) at different temperature (4, 25, 30, 37, 45 °C) for 5 min.

The rest reaction steps were following the abovementioned method by using Catalase Assay Kit.

Resistance ability Measurement

UOx-$Au_{24}Cu_1$@ZIF-8 (the final concentration of the UOx is 0.1mg/mL) was added to PBS (50 mM, pH 8.0) at different temperatures (4, 10, 25, 30, 37, 45 °C). After incubation at specific temperature for 30 min, the catalytic degradation of UA was detected at 292 nm by a UV-vis spectrophotometer. Before the activity test, the mixture will be suspended in solution. The effect of temperature on catalytic activity of UOx-$Au_{24}Cu_1$ were consistent with the above method. The final concentration of UOx and $Au_{24}Cu_1$ in UOx-$Au_{24}Cu_1$ is equal to that in UOx-$Au_{24}Cu_1$@ZIF-8).

The optimum reaction pH of the UOx-$Au_{24}Cu_1$ and UOx-$Au_{24}Cu_1$@ZIF-8 for UA degradation were evaluated by studying catalytic activity of UOx-$Au_{24}Cu_1$ and UOx-$Au_{24}Cu_1$@ZIF-8 in PBS (50 mM) with different pH (pH 7.0-12) at 37°C. The other reaction steps were similar to the above temperature resistance experiment.

UOx-$Au_{24}Cu_1$ or UOx-$Au_{24}Cu_1$@ZIF-8 was dispersed in PBS (50 mM, pH 8.0), then added into trypsin aqueous solutions (0.3 mg/mL). After incubation for 0-50 min at 37 °C, the rest reaction steps were similar to the process above mentioned.

First, by compare the initial value and residual value of the characteristic peak of UA at 292 nm to obtain the degradation amount (Δ292 nm). The highest degradation amount was regard as corresponding control and to be 100% in each experimental condition. The relative activity (%) was calculated using Eq. 7:

$$\text{Relative activity (\%)} = \frac{\Delta 292 \text{ nm in each sample}}{\Delta 292 \text{ nm in control}} \times 100$$

Measurement of UA Degradation

The typical assay contained UOx-$Au_{24}Cu_1$@ZIF-8 (the final concentration of the UOx is 0.1 mg/mL) and 100 μM UA in PBS buffer (50 mM, pH 8.0) at 37 °C. The catalytic efficiency of UA degradation was monitored by measuring the changes of absorbance at 292 nm every 5 min after shaking using a UV-Visible spectrophotometer.

The catalytic activity of UOx, $Au_{24}Cu_1$, UOx-$Au_{24}Cu_1$, $Au_{24}Cu_1$@ZIF-8, and UOx@ZIF-8 were determined by the same method (UOx and $Au_{24}Cu_1$ amount in these samples are equal to that of UOx-$Au_{24}Cu_1$@ZIF-8). The degradation of UA was calculated by the following Eq. 8:

Δ 292 nm=A^t_{292}- A^0_{292}

where A^0_{292} and A^t_{292} represent the characteristic absorbance of UA initially and after reaction (at specific time), respectively.

Detection of accumulated H_2O_2 after UA Degradation

The reaction mixture contained UOx@ZIF-8 or UOx-$Au_{24}Cu_1$@ZIF-8 (the final concentration of the UOx is 0.1mg/mL) and 100 μM UA in PBS buffer. After reaction for a specific time (0-10 min) at 37 °C, UOx@ZIF-8 or UOx-$Au_{24}Cu_1$@ZIF-8 composite was removed using a filter with a size of 13 nm. Then, the pH value of the obtained supernatant was adjusted to 6.0. HRP (1.2 μL, 8 mg/mL) as catalyst and TMB (3 μL, 10 mM) as chromogenic substrate were added into 150 μL of above solution. The reaction sustained for 2 min before terminating by adding 150 μL 1 M H_2SO_4. The absorbance of these solution was recorded at 450 nm corresponding to H_2O_2 amount in a 96-well plate on a PerkinElmer EnSight HH3400 UV-VIS Spectrophotometer. The catalytic activity of UOx, $Au_{24}Cu_1$, UOx-$Au_{24}Cu_1$, and $Au_{24}Cu_1$@ZIF-8 were determined by the same method (UOx and $Au_{24}Cu_1$ amount in these samples are equal to that of UOx-$Au_{24}Cu_1$@ZIF-8).

Stability Measurement

UOx-$Au_{24}Cu_1$ or UOx-$Au_{24}Cu_1$@ZIF-8 was dispersed into deionized water and acquired at given time to test the residual enzymatic activity, which was determined by detecting the typical peak of UA at 292 nm in the reaction system after catalyzed by the sample for 50 min. The initial activity of UOx-$Au_{24}Cu_1$@ZIF-8 was regarded as corresponding control and to be 100% in this experiment. The relative activity (%) was calculated using the following Eq. 7.

Reusability study

For the recycling study, UOx-$Au_{24}Cu_1$@ZIF-8 and UOx-$Au_{24}Cu_1$ (the final concentration of the UOx is 0.1 mg/mL), and 100 μM UA were contained in PBS buffer (50 mM, pH 8.0). After reaction for 10 min, the absorbance of the mixture was detected at 292 nm by a UV-vis spectrophotometer. Before the reaction process was repeated, the recovered composite was obtained by centrifugation and then the supernatant was removed. The degradation of UA was calculated following Eq. 8. The relative activity was calculated as a ratio of each cycle's catalytic activity and first cycle's catalytic activity.

2. Supporting Figures and Tables

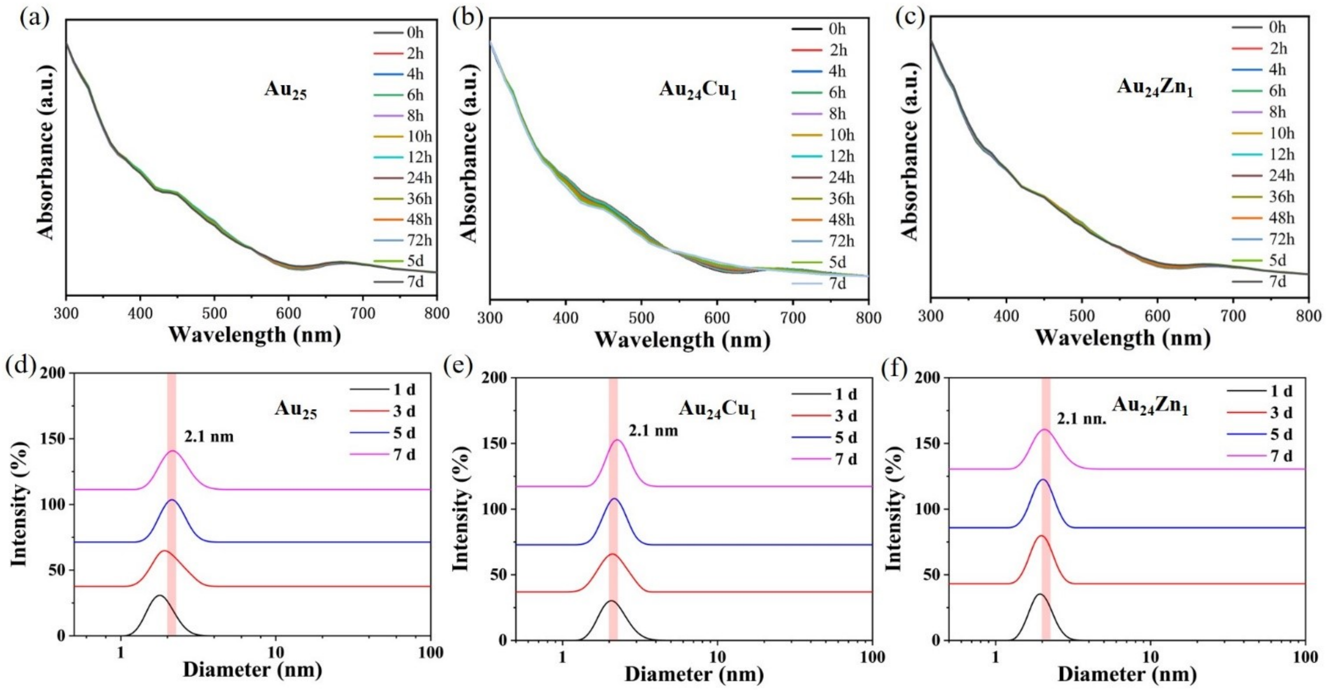

Fig. S1. Stability test of $Au_{24}M_1$ with UV-Vis. UV-vis spectra of (a) Au_{25}, (b) $Au_{24}Cu_1$ and (c) $Au_{24}Zn_1$ dissolved in H_2O under 4℃ and dark conditions for one week. The UV-vis absorption spectra of Au_{25}, $Au_{24}Cu_1$, and $Au_{24}Zn_1$ didn't change significantly after 7 days in water, indicating the satisfied stability of these clusters. Hydrodynamic diameter of (d) Au_{25}, (e) $Au_{24}Cu_1$ and (f) $Au_{24}Zn_1$ was determined at specific time by dynamic light scattering (DLS) in ultrapure water.

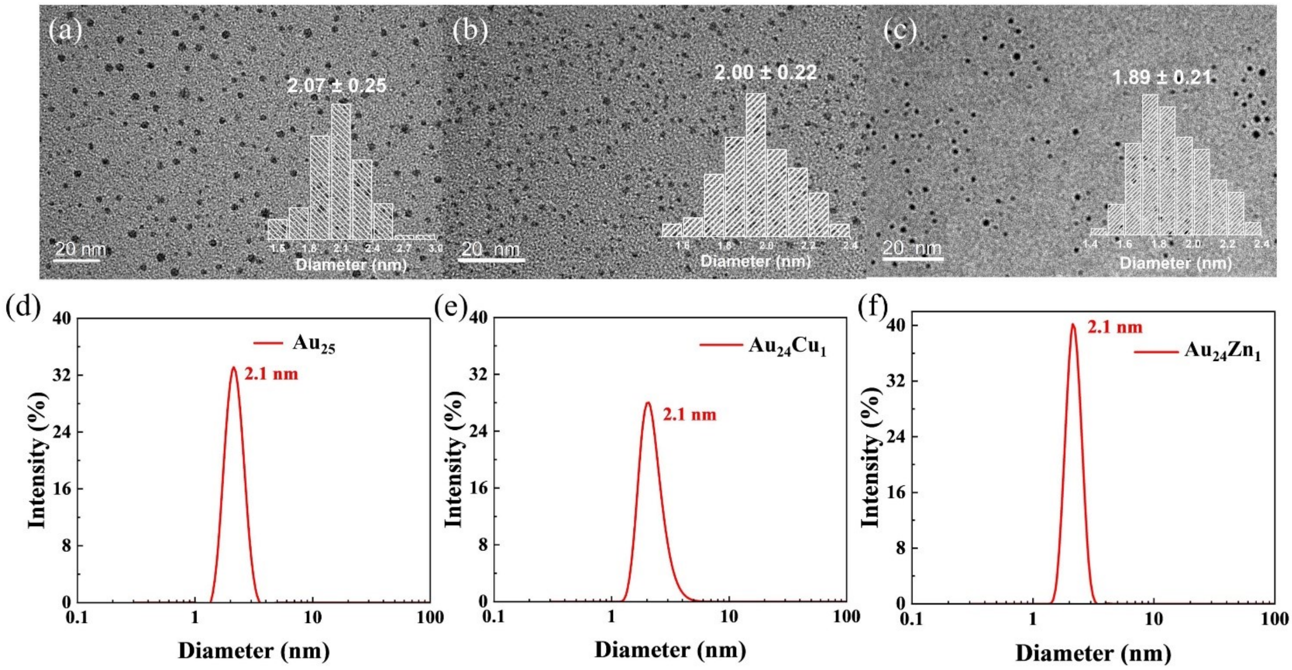

Fig. S2. TEM images of (a) Au_{25}, (b) $Au_{24}Cu_1$ and (c) $Au_{24}Zn_1$. The inset in each figure is the size distribution of clusters analyzed by Image J. Hydrodynamic diameter of (d) Au_{25}, (e) $Au_{24}Cu_1$ and (f) $Au_{24}Zn_1$ was determined by DLS in ultrapure water.

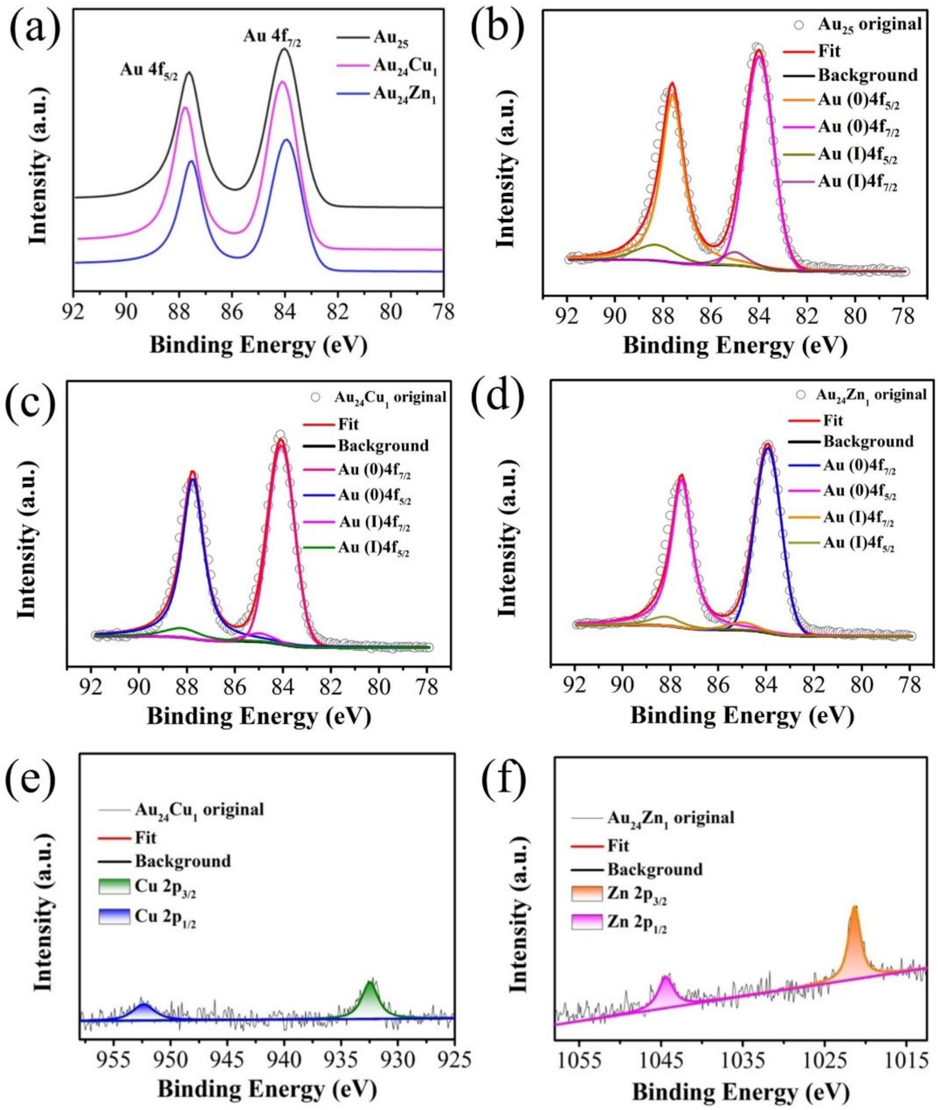

Fig. S3. (a) X-ray photoelectron spectroscopy. Au 4f region of each sample. The high-resolution original and fitted Au 4f region of (b) Au_{25}, (c) $Au_{24}Cu_1$ and (d) $Au_{24}Zn_1$ clusters. Cu 2p XPS spectrum of (e) $Au_{24}Cu_1$ and Zn 2p spectrum of (f) $Au_{24}Zn_1$. All binding energies were calibrated with a C 1s peak of 284.8 eV. Cu 2p peaks (Cu $2p_{3/2}$ =932.5 eV, Cu $2p_{1/2}$ =952.4 eV) were observed. Zn 2p peaks (Zn $2p_{3/2}$ =1021.3 eV, Zn $2p_{1/2}$ =1044.3 eV) were observed. The X-ray photoelectron spectroscopy (XPS) spectrum indicated that mix valence state of Au, including Au (0) and Au (I) existed in all clusters. Besides, the binding energy of 932.5 eV (Cu $2p_{3/2}$) and 952.4 eV (Cu $2p_{1/2}$) indicated the presence of Cu (I),[7, 8] which was probably formed by the reduction of Cu^{2+} during the preparation.

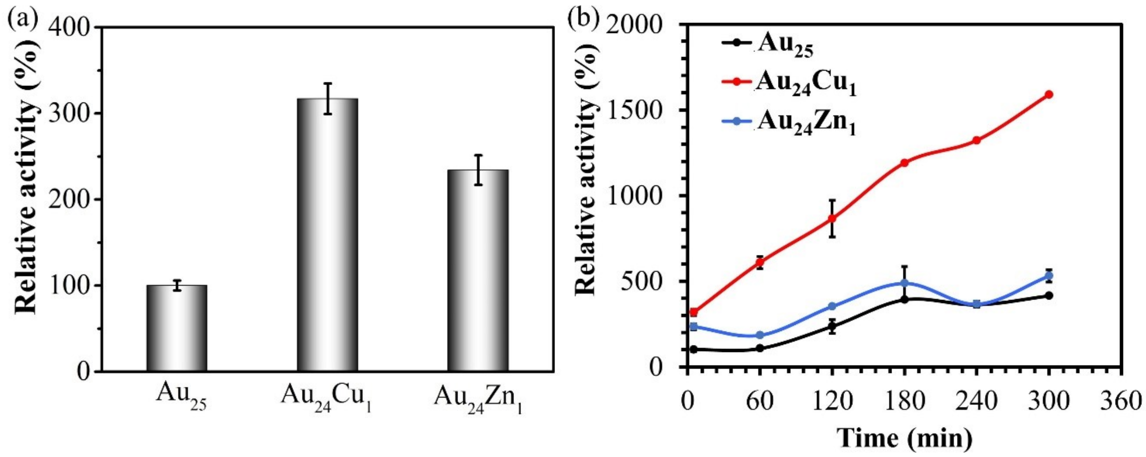

Fig. S4. CAT-like activities of Au_{25}, $Au_{24}Cu_1$ and $Au_{24}Zn_1$. (a) Comparison of the CAT-like capacities of Au NCs after reaction for 5 min. (b) The consumption concentration of H_2O_2 facilitated by Au NCs as a function of reaction time. The catalytic activity of AuNCs was studied by using Catalase Assay Kit. with a characteristic peak at 520 nm.

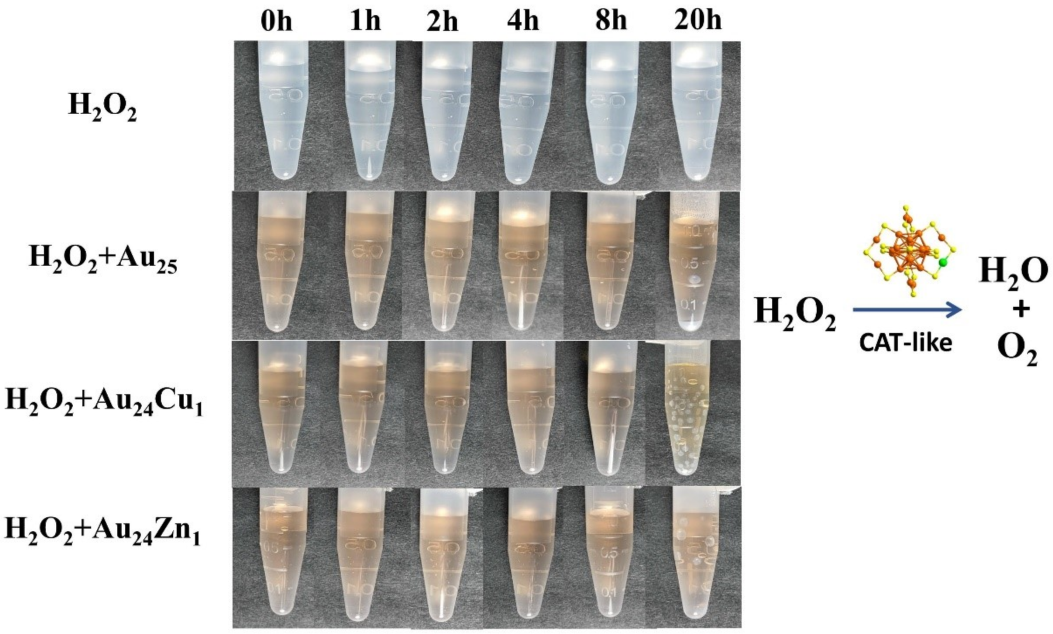

Fig. S5. Photographs of Au_{25}, $Au_{24}Cu_1$ and $Au_{24}Zn_1$ reacting with H_2O_2 at different times. Abundant bubbles were observed in the system under catalysis by $Au_{24}Cu_1$ compared with other two AuNCs, which was in accordance with former results.

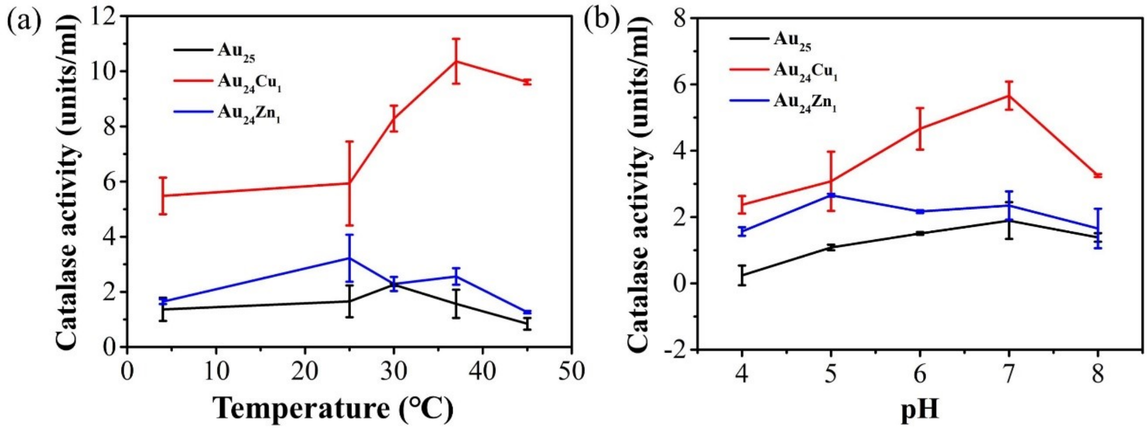

Fig. S6. CAT-like activities of Au_{25}, $Au_{24}Cu_1$ and $Au_{24}Zn_1$ in different (a) temperature and (b) pH values. The optimum temperature and pH value for CAT-like activity of $Au_{24}Cu_1$ was about 37°C and 7, respectively.

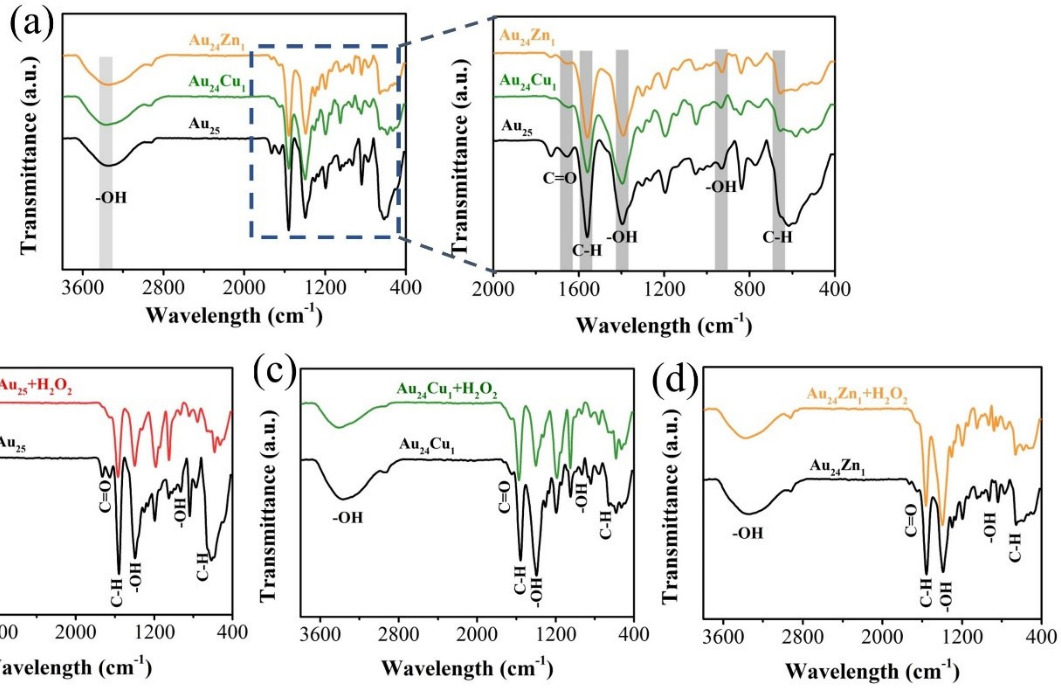

Fig. S7. Fourier-transform infrared (FT-IR) spectra of Au_{25}, $Au_{24}Cu_1$ and $Au_{24}Zn_1$ clusters (a) before and (b-d) after the reaction with H_2O_2. The inset in figure a is a magnification of the FT-IR spectra between 400~2000 cm^{-1}. Considering that the catalytic performance can be affected by the structure, we determined FT-IR spectra of AuNCs. The infrared vibration peak does not change significantly before and after the reaction of H_2O_2, indicating that the ligand structure basically maintain.

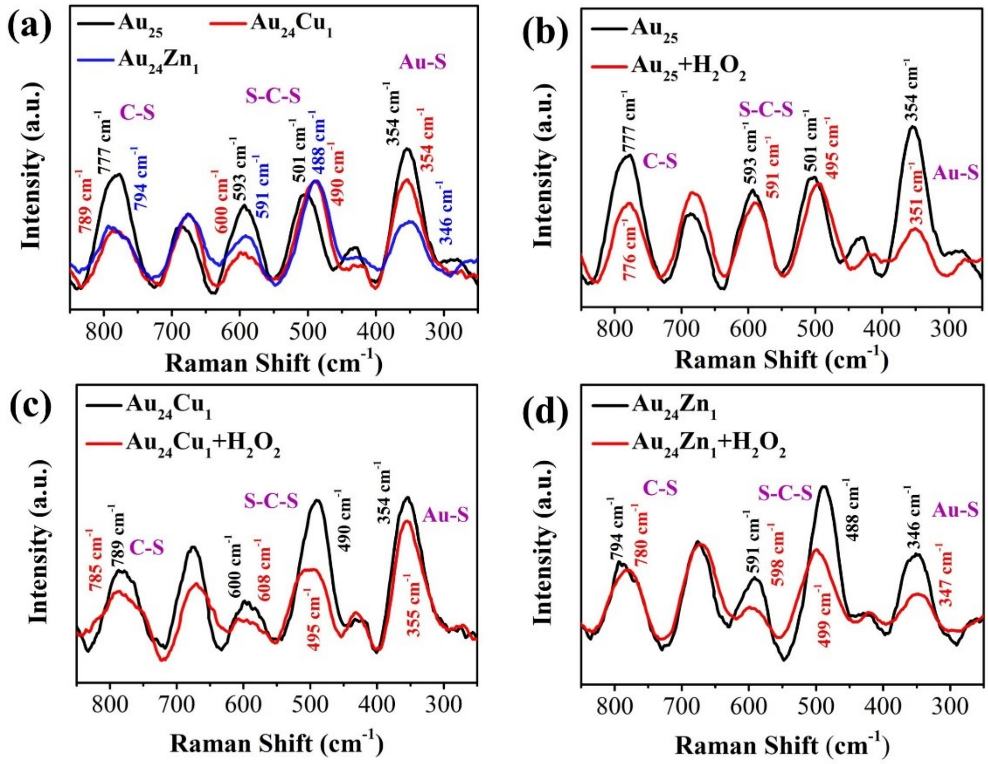

Fig. S8. Raman spectra of Au_{25}, $Au_{24}Cu_1$ and $Au_{24}Zn_1$ clusters (a) before and (b-d) after the reaction with H_2O_2. Negligible changes were observed in the Raman peaks of Au_{25}, $Au_{24}Cu_1$ and $Au_{24}Zn_1$ clusters before and after the reaction with H_2O_2, indicating that the structure of these cluster hardly changed.

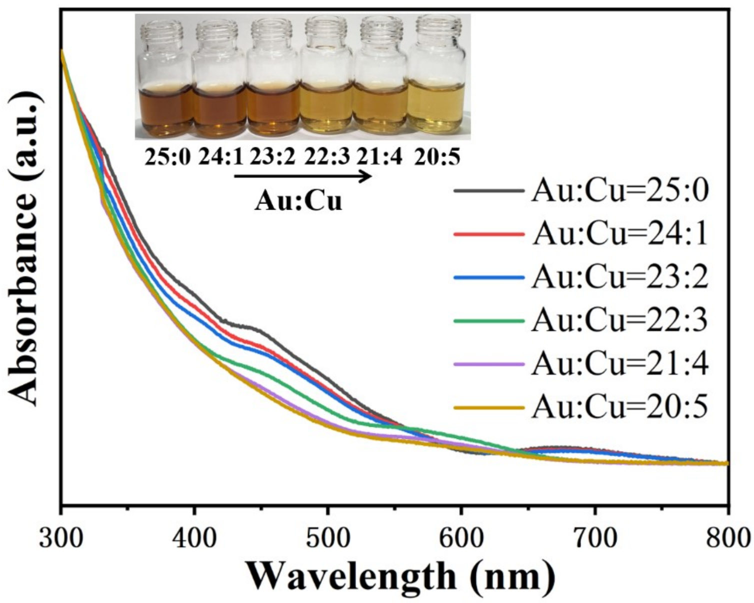

Fig. S9. UV-Vis absorption spectra of Au_{25} substituted with different molar concentrations of Cu (Au:Cu=25:0, 24:1, 23:2, 22:3, 21:4, 20:5). The inset in Figure S9 is the photos of $Au_{25-x}Cu_x$ (x=0-5). Different molar concentrations of Cu were doped into Au_{25} to synthesize $Au_{25-x}Cu_x(MPA)_{18}$ (donated as $Au_{25-x}Cu_x$, x=0-5), in which the molar concentrations between Au and Cu were 25:0, 24:1, 23:2, 22:3, 21:4, and 20:5, respectively. Synthesis process of $Au_{25-x}Cu_x$ (x=1-5) was following the same method as Au_{25} by replacing the Au atoms with nitrate metal ion (Cu^{2+}) at a serious molar ratio. Au_{25}, $Au_{24}Cu_1$, and $Au_{23}Cu_2$ all exhibited the characteristic peaks at approximately 450 nm and 670 nm, confirming their similar structure. However, the characteristic peaks at 450 nm and 670 nm disappeared in other samples, in which the ratio of raw materials containing Au and Cu were 22:3, 21:4, and 20:5, indicating that their structure were different from Au_{25}. Thus, we compared the stability and CAT-like activity of Au_{25}, $Au_{24}Cu_1$ and $Au_{23}Cu_2$ subsequently.

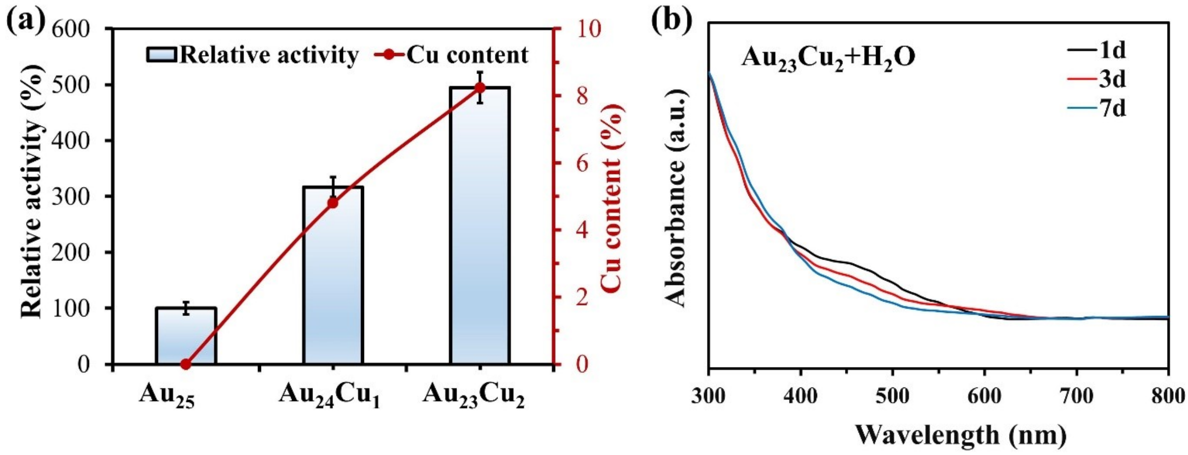

Fig. S10. (a) Comparison of the CAT-like capacities and Cu content of Au_{25}, $Au_{24}Cu_1$ and $Au_{23}Cu_2$. Synthetic process of $Au_{23}Cu_2$ was similar to that of $Au_{24}Cu_1$ with changes of the ratio of raw materials. CAT-like capacities was monitored using Catalase Assay Kit after reaction for 5 min. The Cu content in AuNCs was determined by ICP-MS. (b) Stability test of $Au_{23}Cu_2$ with UV-Vis. UV-vis spectra of $Au_{23}Cu_2$ dissolved in H_2O for 1 day, 3 days and 7 days. The UV-vis absorption spectra of $Au_{23}Cu_2$ disappeared after 3 days in water, indicating the instability of $Au_{23}Cu_2$.

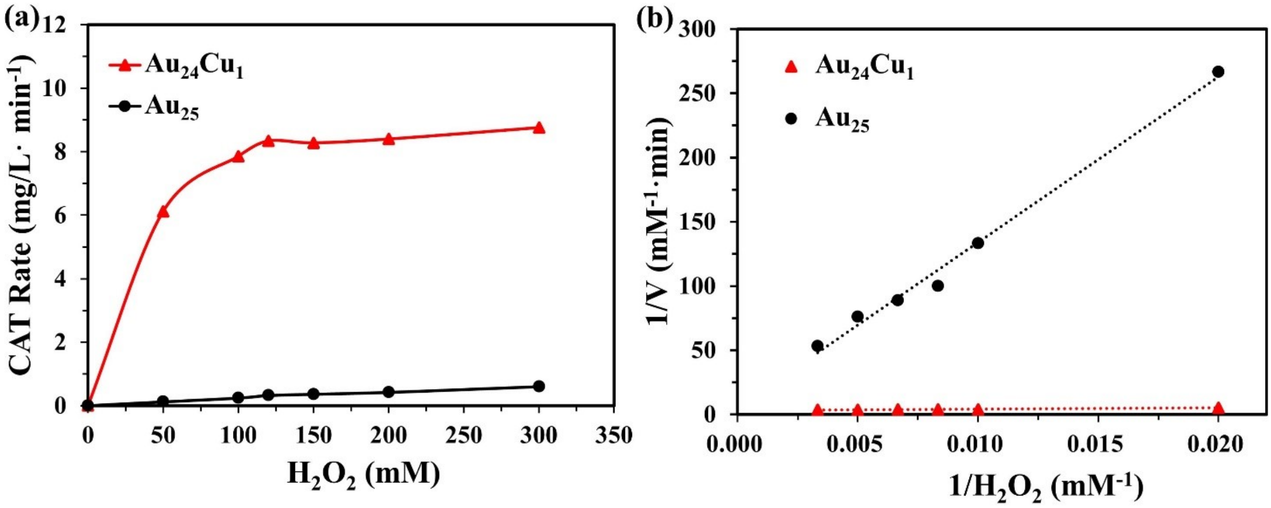

Fig. S11. The reaction kinetic analysis of CAT-like activity of Au_{25} and $Au_{24}Cu_1$. (a) Steady-state kinetic assays of AuNCs (0.5 mg/ml) with CAT-like activity versus vary concentration of H_2O_2 (50–300 mM) at room temperature. (b) Double-reciprocal plots for Au_{25} and $Au_{24}Cu_1$ that were generated from Fig. S11a. The maximum reaction velocity (V_{max}) and Michaelis-Menten constant (K_m) were calculated using the Lineweaver-Burk equation (shown as Eq. 6).

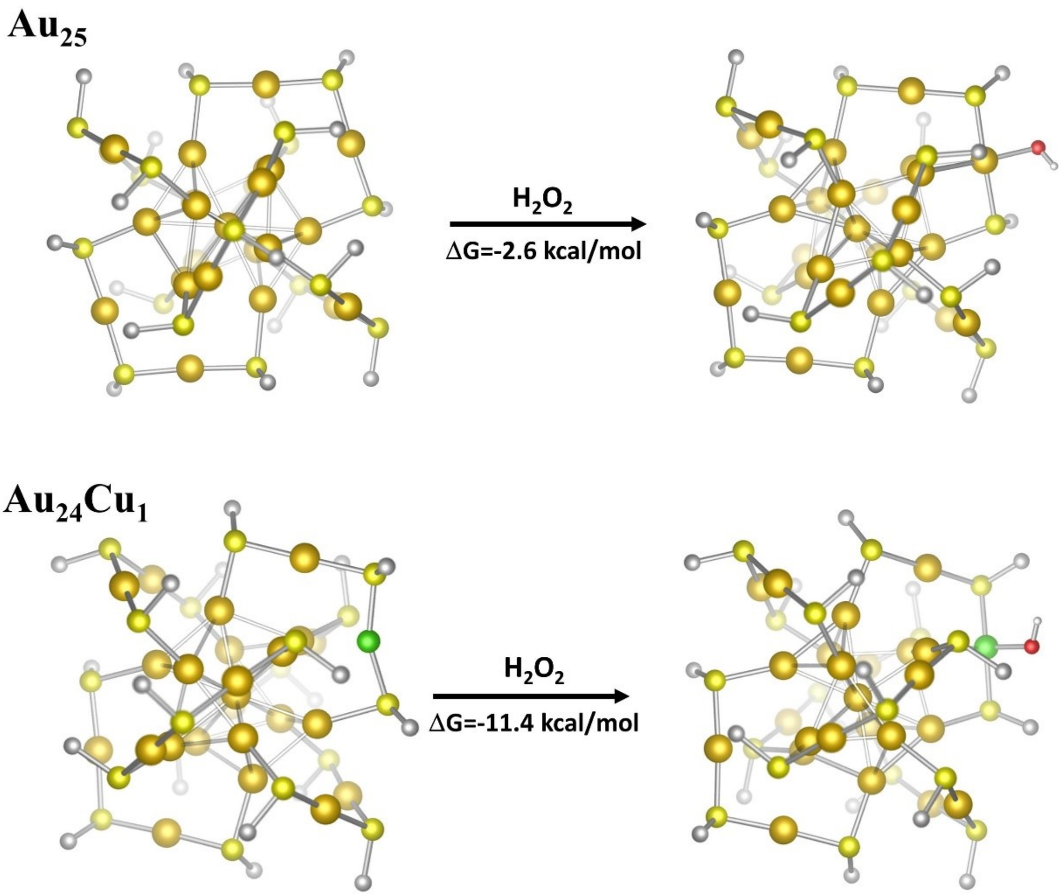

Fig. S12. Formation process and Gibbs free energy of M-OH (M represents metal binding site) in Au_{25} and $Au_{24}Cu_1$. To simply the calculation process, -SMe group replaced the -SR group in MPA ligand. Key: orange = Au; yellow = S; green = Cu; Red = O; dark brown = -Me.

In order to obtain the further view for the CAT-like activity, the density functional theory (DFT) calculation have been performed for the Au_{25} and the $Au_{24}Cu_1$. The critical thermodynamic parameter for the formation of Au-OH in Au_{25} and the Cu-OH in $Au_{24}Cu_1$ have been obtained at B3LYP/def2-SVP level.

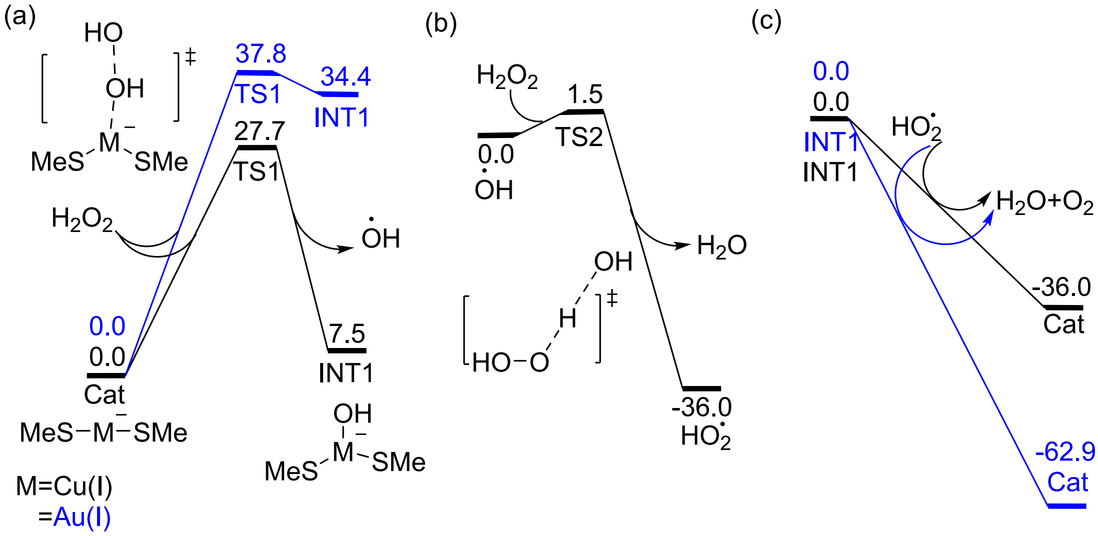

Fig. S13. The whole free energy profiles for the CAT-catalyzed reaction:(a) The free energy profile for the activation of H_2O_2 (b) The transformation between the OH radical and H_2O_2 (c) The generation of oxygen and regeneration of the catalyst. Transition state, donated as TS; intermediate, donated as INT.

According to the general mechanism for the generation of oxygen catalyzed by the nanoclusters, we recalculated the whole process at the DLPNO-CCSD(t)/def2TZVP+CPCM (water)//B3LYP/def2SVP level. Based on the structure of the nanocluster, we find out the outer layer with the negative charge, which can be regard as the active species reacting with the H_2O_2. Hence, the simply model $M(SMe)_2$ anion have been chosen to reveal the general process. According to the previous reports, there are three stages for the whole reaction. As shown in the Fig. S13a, the $M(SMe)_2$ anion can be oxidized by the H_2O_2 via the OH shift process. The calculated results show the copper (I) can be oxidized via the free energy barrier of 27.7 kcal/mol, which would be lower than that of gold(I) for 10.1 kcal/mol, indicating the copper(I) can decompose the H_2O_2 much faster. As shown in the Fig. S13b, the generated OH radical can react with another H_2O_2 via a low free energy barrier of 1.5 kcal/mol, affording a quite stable HO_2 radical. At the last stage (Fig. S13c), the intermediate hydroxide metal INT1 could abstract a hydrogen atom from the HO_2 radical affording an oxygen and water. Moreover, we find out the new generated O_2 can't form the effectively covalent bond with the metal. So, it could be used in the general degradation of· uric· acid.

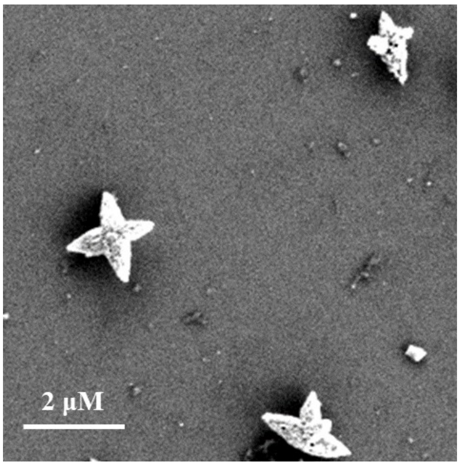

Fig. S14. SEM images of UOx@ZIF-8.

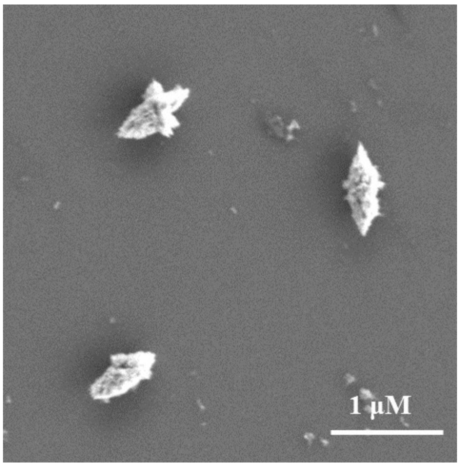

Fig. S15. SEM images of UOx-$Au_{24}Cu_1$@ZIF-8.

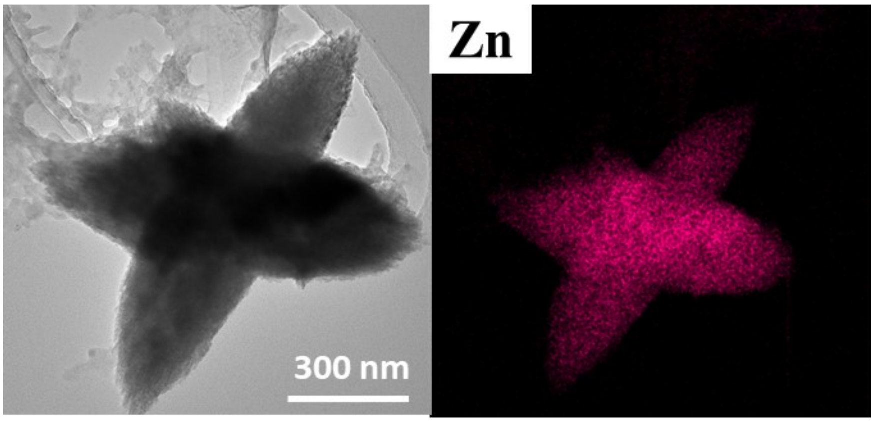

Fig. S16. TEM images and Mapping of UOx@ZIF-8

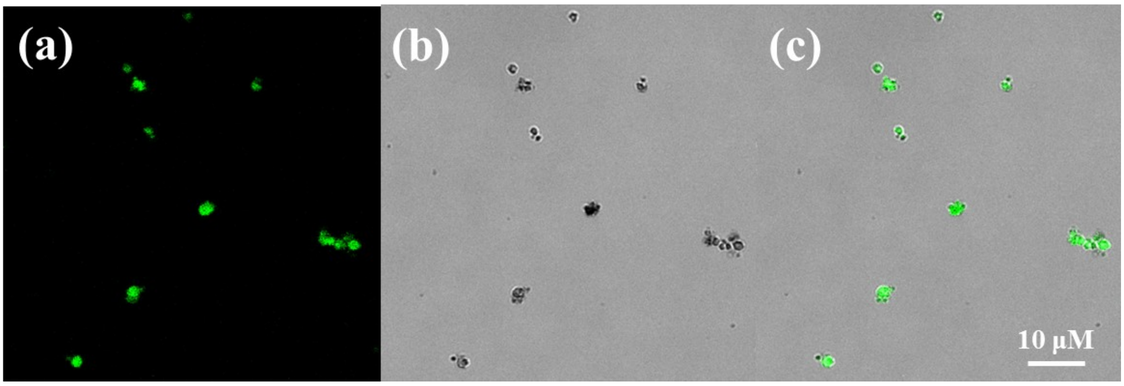

Fig. S17. Confocal laser scanning microscopy image of FITC-labelled UOx in UOx-$Au_{24}Cu_1$@ZIF-8: (a) fluorescent field image of the FITC-UOx, (b) bright-field microscopy image of UOx-$Au_{24}Cu_1$@ZIF-8, and (c) a merged image of UOx-$Au_{24}Cu_1$@ZIF-8. For direct visualization, UOx was labled with fluorescein isothiocyanate (FITC), and then underwent the similar encapsulation process.

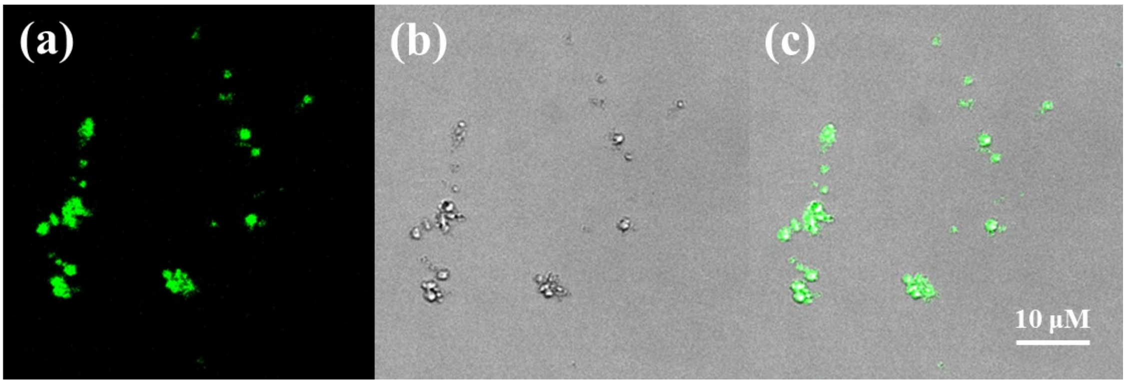

Fig. S18. Confocal laser scanning microscopy image of FITC-labelled UOx in UOx@ZIF-8: (a) fluorescent field image of the FITC-UOx, (b) bright-field microscopy image of UOx@ZIF-8, and (c) a merged image of UOx@ZIF-8.

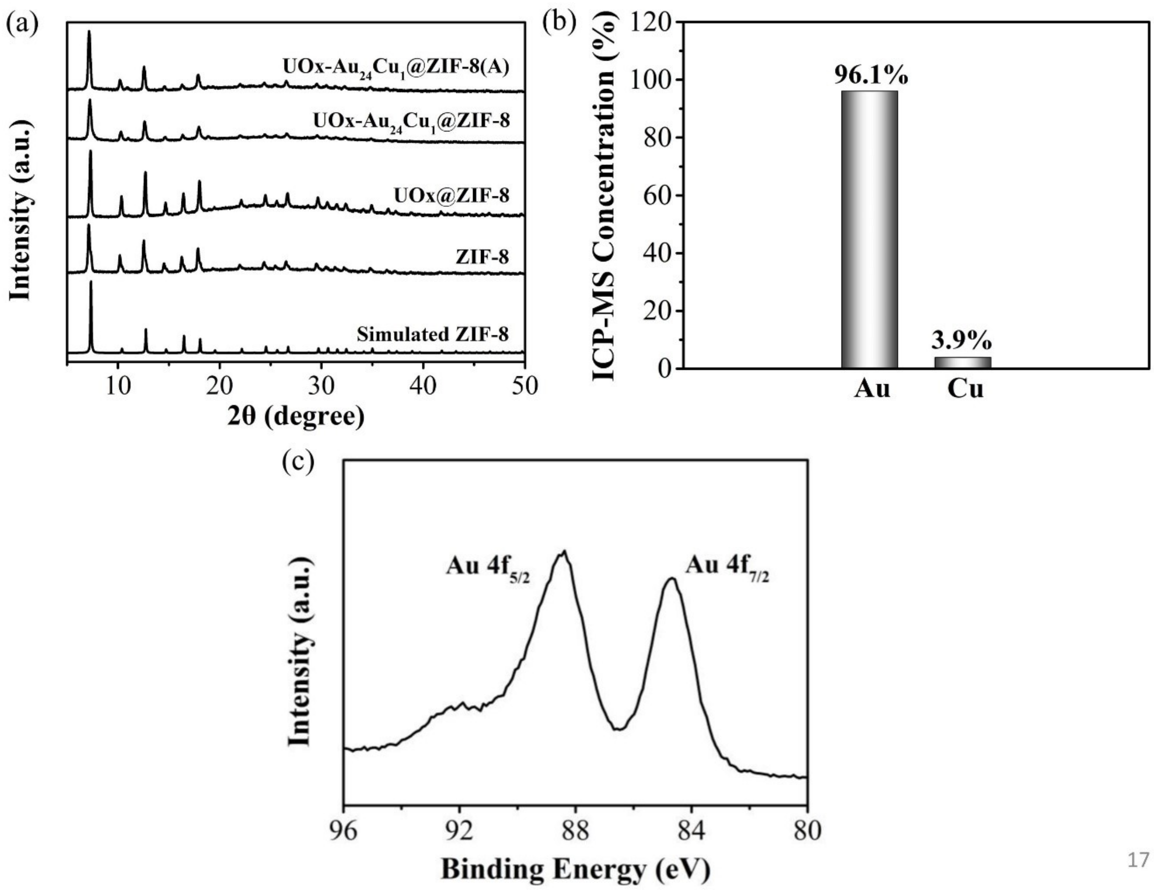

Fig. S19. (a) The powder X-ray diffraction (PXRD) patterns of simulated ZIF-8, pure ZIF-8, UOx@ZIF-8 and UOx-$Au_{24}Cu_1$@ZIF-8 composite (UOx-$Au_{24}Cu_1$@ZIF-8(A) represents that after reaction). The PXRD patterns of UOx@ZIF-8 and UOx-$Au_{24}Cu_1$@ZIF-8 resembled that of the pure ZIF-8 and simulated one, indicating that the crystallinity of ZIF-8 was not significantly affected by the incorporation of enzyme and nanocluster. (b) ICP-MS of UOx-$Au_{24}Cu_1$@ZIF-8. The ICP-MS analysis confirmed the presence of $Au_{24}Cu_1$ in UOx-$Au_{24}Cu_1$@ZIF-8 with the 3.9% ratios of Cu to the total metal belong to $Au_{24}Cu_1$. (c) X-ray photoelectron spectroscopy. Au 4f region of UOx-$Au_{24}Cu_1$@ZIF-8 composite.

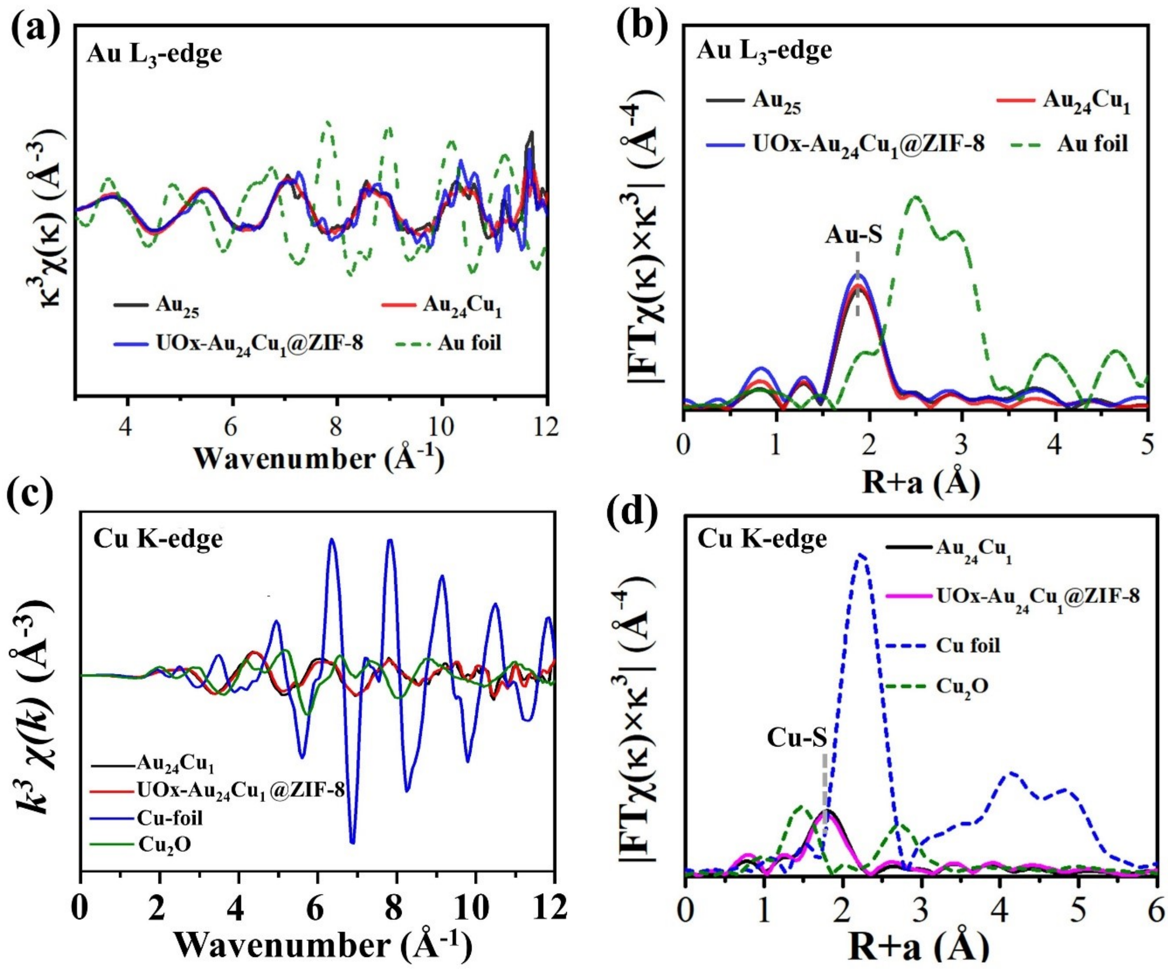

Fig. S20. (a) EXAFS K-space spectra of Au_{25}, $Au_{24}Cu_1$ and UOx-$Au_{24}Cu_1$@ZIF-8 with reference Au-foil at Au L_3-edge. (b) FT-EXAFS spectra in the R-space of Au_{25}, $Au_{24}Cu_1$ and UOx-$Au_{24}Cu_1$@ZIF-8 with reference Au-foil. (c) EXAFS K-space spectra of $Au_{24}Cu_1$ and UOx-$Au_{24}Cu_1$@ZIF-8 with reference materials at Cu k-edge. (d) FT-EXAFS spectra in the R-space of $Au_{24}Cu_1$ and UOx-$Au_{24}Cu_1$@ZIF-8 with reference Cu-foil, Cu_2O.

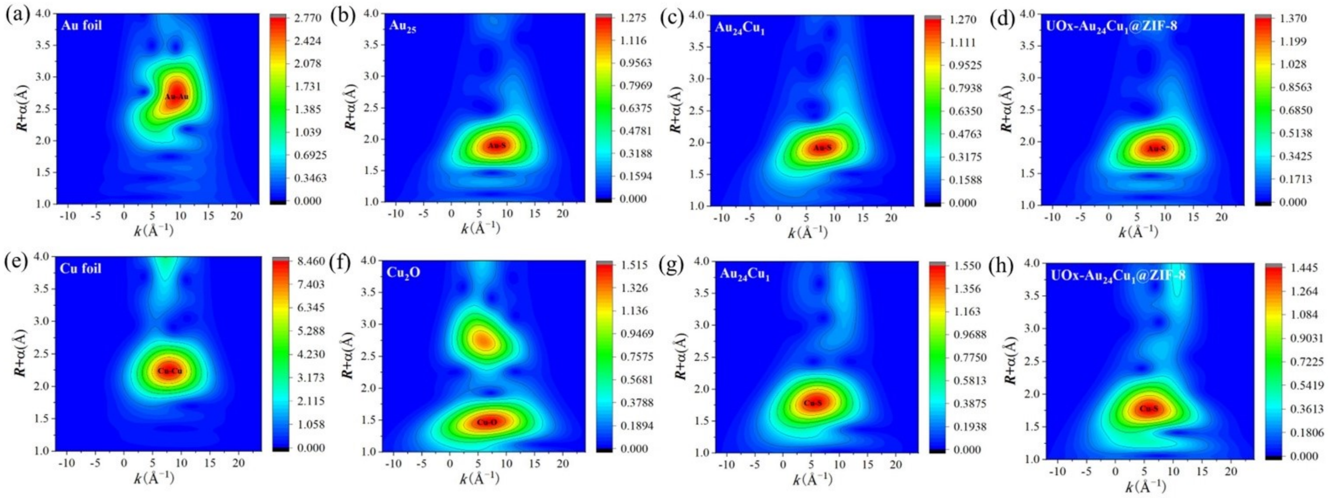

Fig. S21. The wavelet transforms analysis of Au L_3-edge EXAFS for (a) Au foil, (b) Au_{25}, (c) $Au_{24}Cu_1$, (d) UOx-$Au_{24}Cu_1$@ZIF-8. The wavelet transforms analysis of Cu K-edge EXAFS for (e) Cu foil, (f) Cu_2O, (g) $Au_{24}Cu_1$, and (h) UOx-$Au_{24}Cu_1$@ZIF-8.

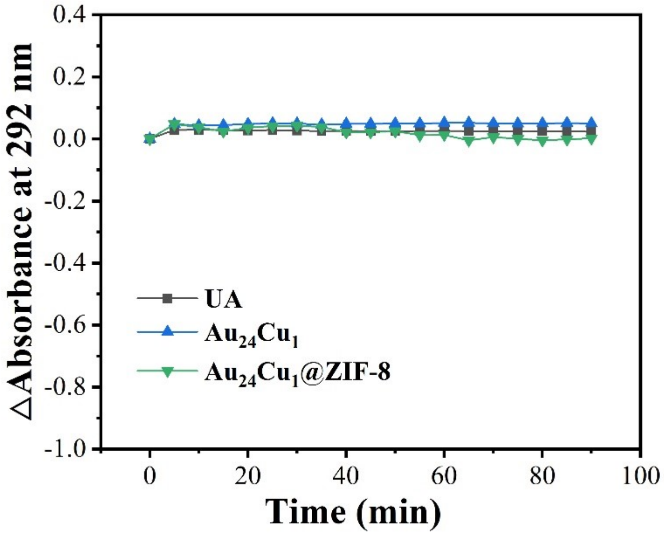

Fig. S22. Time evolution of ΔA_{292} nm corresponding to the degradation of UA (100 μM) catalyzed by $Au_{24}Cu_1$ and $Au_{24}Cu_1$@ZIF-8 ($Au_{24}Cu_1$: 0.2 mg/mL; UOx: 0.1 mg/mL).

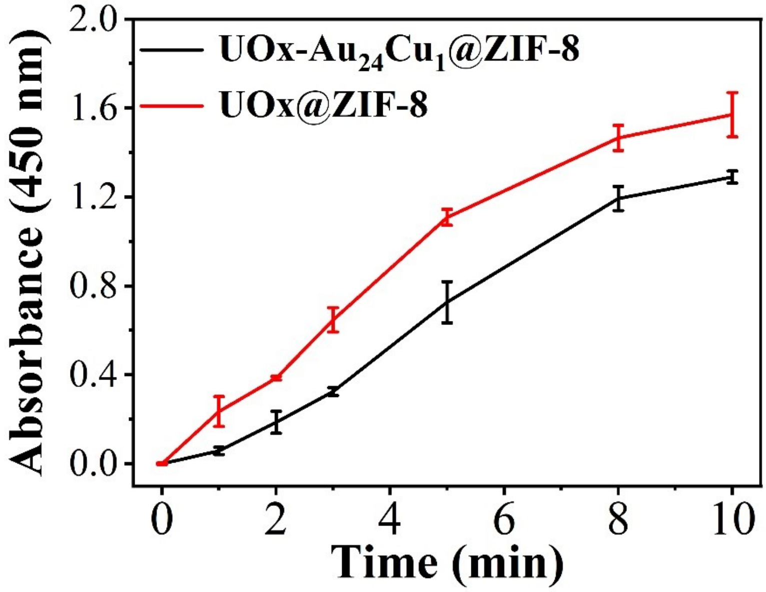

Fig. S23. Simultaneous H_2O_2 generation after UA degradation in the catalytic systems facilitated by UOx@ZIF-8 and UOx-$Au_{24}Cu_1$@ZIF-8 was monitored by detecting the absorbance changes in TMB at 450 nm under HRP catalysis.

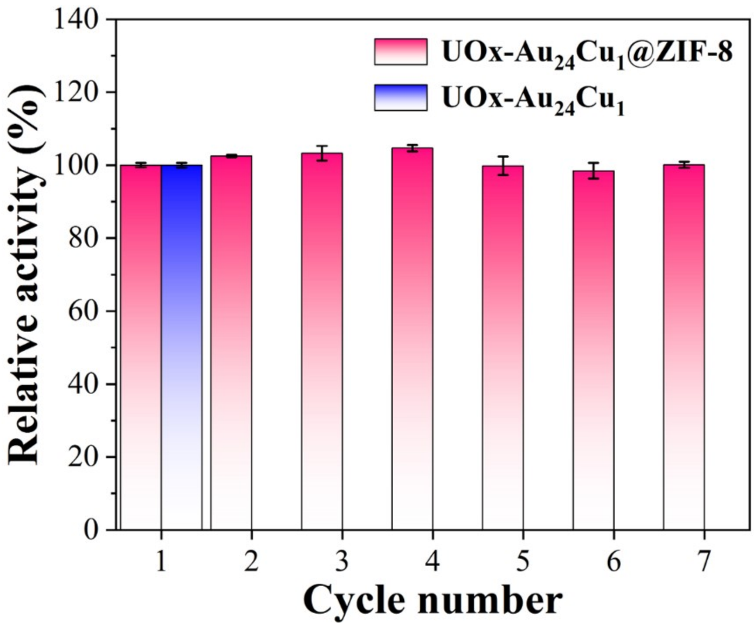

Fig. S24 Reusability of UOx-$Au_{24}Cu_1$@ZIF-8 and UOx-$Au_{24}Cu_1$ in the UA degradation cascade reaction catalytic cycles.

To explore the reusability of the enzyme-nanomaterial cascade system in UA degradation, we have also determined the recycling of UOx-$Au_{24}Cu_1$@ZIF-8 and UOx-$Au_{24}Cu_1$. In recycling tests, UOx-$Au_{24}Cu_1$@ZIF-8 remained nearly 100% of its original catalytic activity after seven cycles, while free UOx-$Au_{24}Cu_1$ lost approximately all of its activity after only one catalytic cycles, indicating the excellent reusability of the constructed self-cascade system.

Table S1. Representative examples of cascade reactions related to UA degradation/detection in different materials

Host materials type	Host materials	Cascade catalytic system	Application	Advantages of host	Reference
MOFs	ZIF-8	UOX-CAT@ZIF-8-RBC	UA degradation	Chemical and thermal stability; high enzyme encapsulation efficiency and biocompatible; moderate synthetic condition; pH-sensitive; adjustable pore size	9
		UOX-CAT@ZIF-8	UA degradation		10
	PCN-222 (Fe)	UOx@PCN-222(Fe)	UA Detection	Peroxidase-like activity; excellent stability; large surface area and high porosity	11
	HP-DUT-5	UOx-HRP@HP-DUT-5	UA Detection	Large mesopore size; high water and pH stability; high load capacity	12
	Th-MOF	Uricase/Th-MOF	UA Detection	Peroxidase-like activity; stability	13
Noble metal nanozyme	Pd-Ru NSs	Pd-Ru/Uricase@RBC	UA degradation	High CAT-like activity; Synthesis under mild reaction conditions	14
Silica	silica layer	MSN-Pt/uricase@Si	UA degradation	Strong resistance capability	15

Table S2. Comparison of Comparison of the Kinetic Parameters of Au_{25} and $Au_{24}Cu_1$, Natural Enzymes, and Other CAT Mimic Materials. *K*m is the Michaelis constant, *V*max is the maximal reaction velocity.

Catalyst	K_m (mM)	V_{max} (mM/min)	Reference
$Au_{24}Cu_1$	29.56	0.31	This work
Au_{25}	655.51	0.059	This work
CAT	54.3	0.97	16
Pd-Ru (11 nm)	31.02	0.26	14
Pd-Ru (30 nm)	29.42	0.22	14
Multi-caged IrOx NPs	187.95	0.34	17
AgPt NP	62.98	0.366	18
PVP-PtNCs	30.62	0.45	19
PVP-PtCuNCs	9.94	1.57	19
N-PCNSs-3	66.25	0.0162	20
Co_3O_4	34.3	0.672	16
Co_3O_4 nanoplates	52.6	0.143	21
Co_3O_4 nanorods	43.3	0.113	21
Co_3O_4 nanocubes	98.1	0.074	21
Pt–Ft	420.60	50.4	22
Fe-SAs/NC	297	0.405	23

Table S3. Formation process and Gibbs free energy of M-OH in Au_{25} and $Au_{24}Cu_1$

Species	Gibbs free energy (a.u.)	Species	Gibbs free energy (a.u.)
H_2O_2	-151.419092	Au_{25}	-11278.97935
H_3O_3	-227.144187	Au_{25}-OH	-11354.67744
$Au_{24}Cu_1$	-12784.14474	$Au_{24}Cu_1$-OH	-12859.85694

Table S4. EXAFS fitting parameters at the Au L_3-edge or Cu K-edge for various samples

Sample	Shell	R(Å)[a]	σ^2(Å^2)[b]	ΔE_0(eV)[c]	R factor
		Au			
Au-foil	Au-Au	2.859±0.003	0.0080±0.0004	3.7±0.3	0.0036
Au_{25}	Au-S	2.307±0.011	0.0061±0.0003	8.7±1.5	0.0098
$Au_{24}Cu_1$	Au-S	2.306±0.011	0.0052±0.0016	8.3±1.4	0.0099
UOx-$Au_{24}Cu_1$@ZIF-8	Au-S	2.299±0.012	0.0011±0.0016	8.9±1.9	0.0157
		Cu			
Cu-foil	Cu-Cu	2.543±0.003	0.0088±0.0004	4.3±0.4	0.0021
	Cu-O	1.843±0.001	0.0023±0.0007	6.5±0.9	
Cu_2O	Cu-Cu	3.070±0.001	0.0249±0.0012	12.8±0.5	0.0064
	Cu-O	3.584±0.001	0.0078±0.0030	4.3±0.4	
$Au_{24}Cu_1$	Cu-S	2.267±0.008	0.0125±0.0012	1.5±0.6	0.0042
UOx-$Au_{24}Cu_1$@ZIF-8	Cu-S	2.260±0.014	0.0134±0.0024	2.1±1.2	0.0169

[a]R, the distance to the neighboring atom; [b]σ^2, the Mean Square Relative Displacement (MSRD); [c]ΔE_0, inner potential correction; R factor indicates the goodness of the fit.

Table S5. The coordination for the species in the calculation

H_2O_2

8	-1.418698000	0.370276000	0.198842000
1	-1.865640000	1.090481000	0.671656000
8	-0.062810000	0.860918000	0.198795000
1	0.384133000	0.140805000	0.671748000

H_3O_3

8	-0.945985000	0.095480000	0.647031000
1	-2.308760000	1.599240000	0.938426000
8	0.184046000	0.648656000	0.268582000
1	0.813478000	-0.093252000	0.136947000
8	-3.006087000	2.256092000	1.096240000
1	-3.757463000	1.712166000	1.366552000

Au_{25}

79	0.087730000	0.024880000	-0.076800000
79	-0.894550000	-0.174150000	2.635560000
79	-2.201590000	1.683320000	0.581730000
79	-2.313660000	-1.521340000	0.440900000
79	2.472650000	1.568000000	-0.636150000
79	-0.280930000	2.560420000	-1.412250000
79	-0.203970000	-2.324150000	-1.813490000
79	-1.816640000	0.046210000	-2.263580000
79	2.424990000	-1.612200000	-0.546770000
79	0.468870000	2.394460000	1.597240000
79	1.048040000	0.246580000	-2.829770000
79	0.355620000	-2.581800000	1.192550000
79	-4.341790000	-0.146790000	2.880030000
79	2.011360000	-0.080240000	2.082850000
79	3.506710000	-3.321090000	2.292120000
79	-0.862970000	-1.738920000	-5.052300000
79	2.449050000	3.268650000	-3.530540000
79	-3.538190000	3.198480000	-2.111600000
79	-3.498270000	-2.835480000	-2.703890000
79	-2.462740000	-3.258880000	3.324010000
79	1.948580000	-4.980230000	-0.614080000
79	1.005140000	1.714660000	4.881940000
79	4.414550000	0.179130000	-3.029520000
79	3.584700000	2.961240000	2.519800000
79	-1.629040000	5.042410000	0.471610000
16	-4.269470000	-2.706650000	-0.457790000
16	4.325120000	2.930590000	0.255960000
16	4.431510000	2.194300000	-4.303030000
16	-3.888520000	1.076120000	-3.114750000
16	3.586700000	-1.303850000	3.548360000
16	-2.894840000	-2.981530000	-5.000590000
16	1.183790000	-0.537800000	-5.200740000
16	-4.417210000	-2.165770000	4.132580000
16	-0.527950000	-4.439870000	2.611900000
16	0.530610000	4.461350000	-2.803110000
16	0.433210000	-4.665890000	-2.421090000
16	-0.913430000	0.322750000	5.069340000
16	3.547140000	-5.380180000	1.105490000
16	2.848980000	3.224100000	4.771170000
16	-4.366300000	1.939600000	1.742860000
16	-3.353420000	5.366840000	-1.145190000
16	4.390040000	-1.955920000	-1.980480000

16	0.218540000	4.850630000	1.956120000
6	2.764750000	-6.585920000	2.257830000
1	2.613830000	-7.527710000	1.712970000
1	3.459080000	-6.752140000	3.092710000
1	1.807380000	-6.208940000	2.640370000
6	-1.216480000	-5.664110000	1.418840000
1	-0.373890000	-6.125290000	0.884170000
1	-1.763880000	-6.432000000	1.982270000
1	-1.886000000	-5.185820000	0.693610000
6	5.295820000	-0.672800000	3.294790000
1	5.624120000	-0.803970000	2.257270000
1	5.311250000	0.395480000	3.551880000
1	5.971390000	-1.225180000	3.962890000
6	5.891880000	-2.055330000	-0.926510000
1	6.770530000	-2.134230000	-1.581580000
1	5.992410000	-1.176700000	-0.278640000
1	5.809730000	-2.961400000	-0.310700000
6	5.819020000	1.859810000	0.255060000
1	6.067330000	1.622250000	-0.788910000
1	6.646950000	2.417140000	0.715180000
1	5.646450000	0.930310000	0.808240000
6	-4.921910000	5.550340000	-0.196800000
1	-5.112550000	4.676370000	0.438850000
1	-4.845880000	6.458020000	0.417200000
1	-5.741110000	5.665250000	-0.919660000
6	-0.561160000	4.578710000	-4.278750000
1	-1.514770000	5.016680000	-3.952910000
1	-0.085690000	5.240330000	-5.015710000
1	-0.744750000	3.594740000	-4.727910000
6	-0.443700000	5.155670000	3.644920000
1	0.383180000	5.014400000	4.354110000
1	-0.796880000	6.194730000	3.697450000
1	-1.261890000	4.470040000	3.895370000
6	4.136770000	2.453620000	5.837230000
1	4.289090000	1.396090000	5.588770000
1	5.073240000	3.012240000	5.704610000
1	3.803900000	2.540810000	6.880580000
6	-0.288780000	-1.198690000	5.899090000
1	0.642630000	-1.554100000	5.441450000
1	-0.120780000	-0.970850000	6.960540000
1	-1.063600000	-1.972270000	5.804900000
6	5.786580000	3.234600000	-3.613930000
1	5.792580000	4.183740000	-4.167000000
1	5.637490000	3.434810000	-2.545380000
1	6.738940000	2.711470000	-3.775400000
6	0.844250000	0.893600000	-6.304240000
1	-0.035310000	1.460950000	-5.975630000
1	1.728520000	1.545600000	-6.285560000
1	0.683990000	0.520030000	-7.324920000
6	1.553310000	-4.517500000	-3.876590000
1	0.952460000	-4.178450000	-4.732210000
1	2.361580000	-3.799100000	-3.691950000
1	1.977610000	-5.508020000	-4.090510000
6	-3.674690000	1.317270000	-4.925660000
1	-4.513730000	1.921350000	-5.297330000
1	-2.726660000	1.817670000	-5.157990000
1	-3.694320000	0.326710000	-5.400430000
6	-2.397110000	-4.738110000	-5.247270000
1	-3.302380000	-5.355880000	-5.172610000
1	-1.969510000	-4.833970000	-6.254550000

1	-1.667290000	-5.056450000	-4.491680000
6	-4.012080000	3.140590000	3.094390000
1	-4.913440000	3.237590000	3.715110000
1	-3.171060000	2.807820000	3.714910000
1	-3.770330000	4.109100000	2.634330000
6	-5.794170000	-3.145570000	3.396690000
1	-5.822720000	-4.119340000	3.904490000
1	-6.733620000	-2.607960000	3.583860000
1	-5.651480000	-3.294310000	2.318800000
6	-5.636700000	-1.475830000	-0.543850000
1	-6.505620000	-1.965470000	-1.004880000
1	-5.882370000	-1.168720000	0.482450000
1	-5.349440000	-0.597730000	-1.135000000

Au_{25}-OH

79	0.169584000	-0.078751000	0.111654000
79	-1.029555000	-0.402311000	2.674342000
79	-2.166158000	1.701642000	0.739847000
79	-2.330868000	-1.466556000	0.414327000
79	2.663597000	1.261138000	-0.384358000
79	-0.055022000	2.617471000	-1.043247000
79	-0.168300000	-2.494398000	-1.534332000
79	-1.862021000	0.552022000	-1.908635000
79	2.488431000	-1.702793000	-0.523065000
79	0.521833000	2.494716000	1.924746000
79	1.230272000	0.189628000	-2.543171000
79	0.274774000	-2.717236000	1.311253000
79	-4.289815000	-0.272936000	3.079777000
79	2.081104000	0.310025000	2.548909000
79	3.442420000	-3.372570000	2.079705000
79	-1.059123000	-1.695689000	-4.826743000
79	2.770010000	3.137820000	-3.253205000
79	-3.935329000	3.190312000	-2.125055000
79	-3.636249000	-2.845225000	-2.638625000
79	-2.360356000	-3.417110000	3.534895000
79	1.921613000	-5.089596000	-0.777142000
79	1.006030000	2.002116000	4.650342000
79	4.567559000	-0.127733000	-3.003928000
79	3.774013000	3.037439000	2.429103000
79	-2.092741000	4.986009000	0.462530000
16	-4.328055000	-2.652659000	-0.384852000
16	4.626623000	2.626165000	0.248942000
16	4.601835000	1.935724000	-4.202444000
16	-3.860475000	1.083272000	-3.221280000
16	3.353842000	-1.532877000	3.560601000
16	-3.057879000	-2.976025000	-4.936013000
16	0.959443000	-0.463455000	-4.877005000
16	-4.376834000	-2.357167000	4.228124000
16	-0.363225000	-4.543897000	2.881208000
16	1.041457000	4.456928000	-2.296777000
16	0.294078000	-4.734698000	-2.480260000
16	-0.878165000	0.499189000	4.928394000
16	3.647375000	-5.393695000	0.825263000
16	2.763392000	3.657091000	4.477162000
16	-4.280557000	1.878662000	2.060013000
16	-3.978877000	5.263869000	-0.977944000
16	4.435591000	-2.274415000	-1.980918000
16	-0.129066000	4.946319000	1.784792000
6	3.070078000	-6.690463000	2.000074000
1	2.952231000	-7.629652000	1.442806000

1	3.845253000	-6.814389000	2.768491000
1	2.122000000	-6.408187000	2.475095000
6	-1.005606000	-5.855800000	1.754776000
1	-0.153234000	-6.280814000	1.205561000
1	-1.479952000	-6.637091000	2.364510000
1	-1.730656000	-5.453932000	1.036454000
6	5.088897000	-0.975943000	3.798618000
1	5.575905000	-0.727959000	2.847873000
1	5.070397000	-0.087247000	4.443864000
1	5.646545000	-1.778953000	4.299594000
6	5.955417000	-2.490618000	-0.970596000
1	6.820176000	-2.550805000	-1.645833000
1	6.094515000	-1.664327000	-0.262967000
1	5.855215000	-3.435046000	-0.418126000
6	5.992523000	1.412673000	0.455976000
1	6.279278000	1.062952000	-0.546045000
1	6.845295000	1.916555000	0.931251000
1	5.680673000	0.554288000	1.062473000
6	-5.456227000	5.142772000	0.117801000
1	-5.448984000	4.212207000	0.699878000
1	-5.450566000	6.012295000	0.789164000
1	-6.350813000	5.178374000	-0.518534000
6	-0.095038000	4.918447000	-3.667380000
1	-0.951736000	5.444962000	-3.224509000
1	0.436472000	5.594618000	-4.350892000
1	-0.450788000	4.039338000	-4.218797000
6	-0.650207000	5.421908000	3.485350000
1	0.235222000	5.349841000	4.131770000
1	-1.006511000	6.460929000	3.464488000
1	-1.439104000	4.765735000	3.871800000
6	3.848243000	3.181593000	5.881022000
1	4.422431000	2.274949000	5.655851000
1	4.530091000	4.022814000	6.067789000
1	3.181187000	3.012309000	6.738109000
6	-0.128414000	-0.778863000	6.016551000
1	0.663946000	-1.327748000	5.492110000
1	0.292937000	-0.261299000	6.887574000
1	-0.930205000	-1.470603000	6.309319000
6	6.072863000	2.854187000	-3.579352000
1	6.105500000	3.823751000	-4.094915000
1	6.015109000	3.016927000	-2.495535000
1	6.971336000	2.275026000	-3.831888000
6	0.589118000	1.060946000	-5.837019000
1	-0.274604000	1.596250000	-5.426106000
1	1.477618000	1.705386000	-5.794024000
1	0.390154000	0.772259000	-6.878031000
6	1.353258000	-4.473587000	-3.967247000
1	0.723313000	-4.060326000	-4.767198000
1	2.181327000	-3.785626000	-3.757097000
1	1.751584000	-5.450185000	-4.274883000
6	-3.387795000	1.440661000	-4.961771000
1	-4.276298000	1.824711000	-5.481708000
1	-2.580453000	2.180208000	-5.019090000
1	-3.066446000	0.498153000	-5.426761000
6	-2.524479000	-4.718629000	-5.211743000
1	-3.422068000	-5.350757000	-5.173161000
1	-2.072951000	-4.784798000	-6.210971000
1	-1.808670000	-5.045247000	-4.446968000
6	-3.916996000	3.010484000	3.465768000
1	-4.789493000	3.033895000	4.132838000

1	-3.032778000	2.681542000	4.025820000
1	-3.742476000	4.012885000	3.049886000
6	-5.694414000	-3.331270000	3.384687000
1	-5.725230000	-4.327287000	3.847016000
1	-6.652700000	-2.820843000	3.551580000
1	-5.498588000	-3.425913000	2.308716000
6	-5.673347000	-1.394916000	-0.460075000
1	-6.561494000	-1.869057000	-0.899361000
1	-5.891619000	-1.072816000	0.567876000
1	-5.378785000	-0.528478000	-1.064251000
8	1.144336000	2.142733000	6.743327000
1	0.233982000	2.253878000	7.057417000

$Au_{24}Cu_1$

79	0.097886000	0.023068000	-0.080472000
79	-0.995773000	-0.297240000	2.586134000
79	-2.259770000	1.663826000	0.467822000
79	-2.364854000	-1.454921000	0.345960000
79	2.516024000	1.503818000	-0.565325000
79	-0.264444000	2.539755000	-1.458848000
79	-0.294130000	-2.252244000	-1.811770000
79	-1.865223000	0.092684000	-2.189990000
79	2.530849000	-1.512070000	-0.373411000
79	0.568477000	2.377445000	1.567531000
79	1.076955000	0.323850000	-2.802539000
79	0.302655000	-2.538063000	1.260129000
79	-4.346050000	-0.230729000	2.907230000
79	2.030443000	-0.052462000	2.064390000
79	3.554070000	-3.252309000	2.341685000
79	-0.959339000	-1.724231000	-5.035149000
79	2.443114000	3.322194000	-3.488515000
79	-3.550086000	3.140651000	-2.135287000
79	-3.628571000	-2.837357000	-2.710794000
79	-2.460270000	-3.363031000	3.312884000
79	2.012637000	-4.848582000	-0.577820000
79	1.024318000	1.821301000	4.744727000
79	4.396677000	0.164065000	-3.062407000
79	3.726225000	2.993167000	2.457587000
16	-4.362673000	-2.740382000	-0.462273000
16	4.467599000	2.902030000	0.209684000
16	4.395699000	2.212933000	-4.287345000
16	-3.938777000	1.060285000	-3.191538000
16	3.529338000	-1.286364000	3.658318000
16	-3.004332000	-2.950268000	-5.003085000
16	1.112643000	-0.582594000	-5.134596000
16	-4.411577000	-2.272507000	4.120809000
16	-0.488378000	-4.487547000	2.646723000
16	0.560933000	4.533548000	-2.710674000
16	0.441126000	-4.545128000	-2.322659000
16	-0.957271000	0.535215000	4.930687000
16	3.659144000	-5.269620000	1.088633000
16	2.850771000	3.353549000	4.640296000
16	-4.358444000	1.868963000	1.806034000
16	-3.218596000	5.245230000	-1.076054000
16	4.263602000	-1.991732000	-2.079936000
16	0.138605000	4.766050000	1.764915000
6	2.882419000	-6.530642000	2.229492000
1	2.747171000	-7.460721000	1.660847000
1	3.588988000	-6.703561000	3.052827000
1	1.921465000	-6.185717000	2.632514000

6	-1.151138000	-5.717330000	1.401437000
1	-0.299573000	-6.167574000	0.871484000
1	-1.701028000	-6.496154000	1.947330000
1	-1.814494000	-5.234261000	0.673617000
6	5.264241000	-0.618276000	3.476298000
1	5.635259000	-0.720250000	2.449724000
1	5.262661000	0.444139000	3.756039000
1	5.916532000	-1.182286000	4.157512000
6	5.860348000	-2.233625000	-1.149915000
1	6.674266000	-2.307700000	-1.884406000
1	6.060178000	-1.407357000	-0.457261000
1	5.784164000	-3.175673000	-0.589660000
6	5.899813000	1.703893000	0.245872000
1	6.193173000	1.482107000	-0.790157000
1	6.740078000	2.176633000	0.772933000
1	5.622818000	0.770337000	0.749665000
6	-4.735701000	5.447636000	-0.025205000
1	-4.960970000	4.535420000	0.542531000
1	-4.557942000	6.286364000	0.662465000
1	-5.585956000	5.689368000	-0.677327000
6	-0.554863000	4.703824000	-4.198045000
1	-1.504014000	5.140642000	-3.858072000
1	-0.073467000	5.381868000	-4.915954000
1	-0.746898000	3.734245000	-4.673603000
6	-0.568063000	5.119451000	3.444900000
1	0.247677000	5.085729000	4.179436000
1	-1.001923000	6.129496000	3.429136000
1	-1.337735000	4.391095000	3.724578000
6	4.104089000	2.628838000	5.814937000
1	4.273489000	1.561238000	5.629228000
1	5.044501000	3.185244000	5.702016000
1	3.718093000	2.766809000	6.834287000
6	-0.417552000	-0.944030000	5.936264000
1	0.515744000	-1.372531000	5.550782000
1	-0.279370000	-0.621348000	6.977366000
1	-1.218436000	-1.694228000	5.884036000
6	5.773322000	3.228812000	-3.538002000
1	5.794610000	4.190388000	-4.068989000
1	5.621170000	3.404789000	-2.465298000
1	6.718612000	2.695916000	-3.709192000
6	0.810984000	0.853051000	-6.288178000
1	-0.061760000	1.444626000	-5.985518000
1	1.708676000	1.486481000	-6.270514000
1	0.658116000	0.458833000	-7.302271000
6	1.534219000	-4.407547000	-3.835145000
1	0.914757000	-4.074256000	-4.679291000
1	2.343648000	-3.687381000	-3.664163000
1	1.956388000	-5.398612000	-4.051487000
6	-3.611816000	1.341116000	-5.006954000
1	-4.411999000	1.973264000	-5.415738000
1	-2.639765000	1.822027000	-5.171736000
1	-3.625670000	0.361456000	-5.504432000
6	-2.472094000	-4.729024000	-5.231029000
1	-3.369938000	-5.357994000	-5.159547000
1	-2.040927000	-4.818704000	-6.237421000
1	-1.740257000	-5.041174000	-4.475071000
6	-3.916247000	3.028314000	3.200628000
1	-4.796236000	3.106584000	3.853914000
1	-3.061373000	2.656169000	3.778792000
1	-3.682497000	4.016131000	2.780226000

6	-5.772286000	-3.255809000	3.299716000
1	-5.804337000	-4.236603000	3.793630000
1	-6.720102000	-2.728062000	3.472762000
1	-5.601315000	-3.386738000	2.223460000
6	-5.738140000	-1.470202000	-0.530467000
1	-6.612426000	-1.939486000	-1.002105000
1	-5.988258000	-1.166368000	0.496023000
1	-5.433853000	-0.590256000	-1.110656000
29	-1.576000000	4.604677000	0.318275000

$Au_{24}Cu_1$-OH

79	0.026668000	0.119075000	0.004819000
79	-0.906744000	-0.311969000	2.706924000
79	-2.298424000	1.965885000	0.490802000
79	-2.386962000	-1.539821000	0.434862000
79	2.446920000	1.674762000	-0.566887000
79	-0.374376000	2.924855000	-1.259033000
79	-0.389880000	-2.133234000	-1.729075000
79	-2.040271000	0.121012000	-2.049817000
79	2.608044000	-1.280591000	-0.175473000
79	0.592185000	2.468961000	1.597345000
79	0.762370000	0.714026000	-2.762860000
79	0.246412000	-2.513451000	1.297224000
79	-4.137451000	-0.370130000	2.940283000
79	2.029831000	0.111366000	2.190622000
79	3.534314000	-3.156941000	2.341184000
79	-1.058681000	-1.572245000	-4.919135000
79	2.601747000	3.286003000	-3.460711000
79	-3.479096000	3.213813000	-2.291214000
79	-3.682160000	-2.832580000	-2.613124000
79	-2.296688000	-3.500866000	3.342664000
79	2.050050000	-4.665715000	-0.630197000
79	1.038808000	1.929541000	4.765249000
79	4.353095000	0.125496000	-3.008910000
79	3.748152000	3.026622000	2.502046000
16	-4.406543000	-2.776694000	-0.346956000
16	4.513292000	2.867390000	0.252456000
16	4.535625000	2.135707000	-4.254632000
16	-4.133753000	1.049961000	-2.994615000
16	3.450512000	-1.249915000	3.745353000
16	-3.078374000	-2.840318000	-4.917584000
16	0.954747000	-0.310367000	-5.023831000
16	-4.221779000	-2.399773000	4.191895000
16	-0.330331000	-4.597690000	2.574780000
16	0.776609000	4.611949000	-2.761930000
16	0.436063000	-4.356875000	-2.341807000
16	-0.919313000	0.593921000	4.990004000
16	3.727207000	-5.111292000	1.000120000
16	2.907604000	3.409723000	4.696781000
16	-4.253064000	1.772156000	1.924429000
16	-2.799887000	5.361457000	-1.619869000
16	4.120679000	-1.979335000	-1.939706000
16	0.153491000	4.822557000	1.690509000
6	3.076239000	-6.473577000	2.054898000
1	2.989732000	-7.373835000	1.431545000
1	3.802044000	-6.652001000	2.859895000
1	2.100890000	-6.209794000	2.483491000
6	-0.997958000	-5.772784000	1.321005000
1	-0.148326000	-6.184526000	0.758175000
1	-1.520469000	-6.582936000	1.847661000

1	-1.686113000	-5.275889000	0.626314000
6	5.173901000	-0.604016000	3.740886000
1	5.597669000	-0.586522000	2.730177000
1	5.157705000	0.418414000	4.141411000
1	5.788867000	-1.246037000	4.386488000
6	5.732510000	-2.345472000	-1.133797000
1	6.469847000	-2.533043000	-1.926606000
1	6.070294000	-1.514754000	-0.503023000
1	5.607500000	-3.251333000	-0.525423000
6	5.798797000	1.553113000	0.301462000
1	6.108642000	1.345116000	-0.732775000
1	6.660898000	1.917075000	0.877163000
1	5.409308000	0.631069000	0.751210000
6	-4.325326000	6.232316000	-1.083300000
1	-4.972465000	5.576233000	-0.486822000
1	-4.024395000	7.100230000	-0.480758000
1	-4.870686000	6.561280000	-1.978711000
6	-0.259409000	4.803020000	-4.272590000
1	-1.148482000	5.378167000	-3.983053000
1	0.316614000	5.360059000	-5.023739000
1	-0.565103000	3.831791000	-4.680617000
6	-0.514012000	5.339342000	3.318158000
1	0.043763000	6.239628000	3.615422000
1	-1.576840000	5.572507000	3.156150000
1	-0.369916000	4.551982000	4.068336000
6	4.113368000	2.720290000	5.902844000
1	4.287064000	1.648699000	5.746797000
1	5.056895000	3.272602000	5.795994000
1	3.707870000	2.882580000	6.910907000
6	-0.386842000	-0.824525000	6.038668000
1	0.547878000	-1.267125000	5.672622000
1	-0.250975000	-0.458190000	7.065411000
1	-1.187793000	-1.575973000	6.017465000
6	5.931004000	3.083489000	-3.513054000
1	5.996819000	4.043902000	-4.042225000
1	5.771316000	3.264949000	-2.442392000
1	6.856874000	2.514170000	-3.672075000
6	0.648685000	1.031418000	-6.244254000
1	-0.274618000	1.581266000	-6.023179000
1	1.504688000	1.719412000	-6.203967000
1	0.581881000	0.584026000	-7.245413000
6	1.462651000	-4.175661000	-3.859969000
1	0.804816000	-3.841661000	-4.674201000
1	2.269832000	-3.448453000	-3.713859000
1	1.885306000	-5.160661000	-4.101280000
6	-3.999297000	1.051020000	-4.829910000
1	-4.791627000	1.695591000	-5.234632000
1	-3.019544000	1.413942000	-5.163204000
1	-4.148869000	0.020343000	-5.179585000
6	-2.560010000	-4.574597000	-5.261564000
1	-3.455564000	-5.208387000	-5.207594000
1	-2.144077000	-4.613109000	-6.277518000
1	-1.816145000	-4.921190000	-4.532925000
6	-3.908998000	2.920726000	3.325952000
1	-4.830447000	2.993981000	3.920468000
1	-3.092717000	2.539791000	3.952108000
1	-3.637861000	3.897989000	2.889735000
6	-5.622551000	-3.362586000	3.480337000
1	-5.647936000	-4.340096000	3.980964000
1	-6.551666000	-2.817385000	3.695068000

1	-5.504762000	-3.500635000	2.397720000
6	-5.788979000	-1.558667000	-0.370461000
1	-6.665519000	-2.042845000	-0.822407000
1	-6.012286000	-1.280630000	0.669209000
1	-5.524349000	-0.661065000	-0.942997000
29	-1.751261000	4.770025000	0.352657000
8	-2.925327000	5.498911000	1.688787000
1	-3.817891000	5.621174000	1.342406000

3. References

1. X. Yuan, N. Goswami, I. Mathews, Y. Yu and J. Xie, Enhancing stability through ligand-shell engineering: A case study with Au25(SR)18 nanoclusters, *Nano Research*, 2015, **8**, 3488-3495.
2. H. Liu, Y. Li, S. Sun, Q. Xin, S. Liu, X. Mu, X. Yuan, K. Chen, H. Wang, K. Varga, W. Mi, J. Yang and X.-D. Zhang, Catalytically potent and selective clusterzymes for modulation of neuroinflammation through single-atom substitutions, *Nature Communications*, 2021, **12**, 114.
3. H. Qian, D.-e. Jiang, G. Li, C. Gayathri, A. Das, R. R. Gil and R. Jin, Monoplatinum Doping of Gold Nanoclusters and Catalytic Application, *Journal of the American Chemical Society*, 2012, **134**, 16159-16162.
4. S. Yamazoe, W. Kurashige, K. Nobusada, Y. Negishi and T. Tsukuda, Preferential Location of Coinage Metal Dopants (M = Ag or Cu) in [Au25–xMx(SC2H4Ph)18]− (x ∼ 1) As Determined by Extended X-ray Absorption Fine Structure and Density Functional Theory Calculations, *The Journal of Physical Chemistry C*, 2014, **118**, 25284-25290.
5. Gaussian 16, M. J. Frisch, G. W. Trucks, H. B. Schlegel, G. E. Scuseria, M. A. Robb, J. R. Cheeseman, G. Scalmani, V. Barone, G. A. Petersson, H. Nakatsuji, X. Li, M. Caricato, A. V. Marenich, J. Bloino, B. G. Janesko, R. Gomperts, B. Mennucci, H. P. Hratchian, J. V. Ortiz, A. F. Izmaylov, J. L. Sonnenberg, D. Williams-Young, F. Ding, F. Lipparini, F. Egidi, J. Goings, B. Peng, A. Petrone, T. Henderson, D. Ranasinghe, V. G. Zakrzewski, J. Gao, N. Rega, G. Zheng, W. Liang, M. Hada, M. Ehara, K. Toyota, R. Fukuda, J. Hasegawa, M. Ishida, T. Nakajima, Y. Honda, O. Kitao, H. Nakai, T. Vreven, K. Throssell, J. A. Montgomery, Jr., J. E. Peralta, F. Ogliaro, M. J. Bearpark, J. J. Heyd, E. N. Brothers, K. N. Kudin, V. N. Staroverov, T. A. Keith, R. Kobayashi, J. Normand, K. Raghavachari, A. P. Rendell, J. C. Burant, S. S. Iyengar, J. Tomasi, M. Cossi, J. M. Millam, M. Klene, C. Adamo, R. Cammi, J. W. Ochterski, R. L. Martin, K. Morokuma, O. Farkas, J. B. Foresman, and D. J. Fox, Gaussian, Inc., Wallingford CT, **2016**.
6. C. Y. Legault, CYLview20, Université de Sherbrooke, **2020**. http://www.cylview.org
7. J. H. Wang, R. L. Huang, W. Qi, R. X. Su and Z. M. He, Construction of biomimetic nanozyme with high laccase- and catecholase-like activity for oxidation and detection of phenolic compounds, *J Hazard Mater*, 2022, 429.
8. W. Cheng, H. Zhang, D. Luan and X. W. Lou, Exposing unsaturated Cu1-O2 sites in nanoscale Cu-MOF for efficient electrocatalytic hydrogen evolution, *Science Advances*, 2021, **7**, eabg2580.
9. Z. Li, L. Xue, J. Yang, S. Wuttke, P. He, C. Lei, H. Yang, L. Zhou, J. Cao, A. Sinelshchikova, G. Zheng, J. Guo, J. Lin, Q. Lei, C. J. Brinker, K. Liu and W. Zhu, Synthetic Biohybrids of Red Blood Cells and Cascaded-Enzymes@ Metal–Organic Frameworks for Hyperuricemia Treatment, *Advanced Science*, 2024, 11, 2305126.
10. L. Zhang, C. Zhang, Z.-N. Zhuang, C.-X. Li, P. Pan, C. Zhang and X.-Z. Zhang, Bio-inspired nanoenzyme for metabolic reprogramming and anti-inflammatory treatment of hyperuricemia and gout, *Science China Chemistry*, 2021, 64, 616-628.
11. X. Liang, Y. Chen, K. Wen, H. Han and Q. Li, Urate oxidase loaded in PCN-222(Fe) with peroxidase-like activity for colorimetric detection of uric acid, *J Mater Chem B*, 2021, 9, 6811-6817.
12. X. Liu, W. Qi, Y. Wang, R. Su and Z. He, A facile strategy for enzyme immobilization with highly stable hierarchically porous metal–organic frameworks, *Nanoscale*, 2017, 9, 17561-17570.
13. A. Badoei-dalfard, N. Sohrabi, Z. Karami and G. Sargazi, Fabrication of an efficient and sensitive colorimetric biosensor based on Uricase/ Th-MOF for uric acid sensing in biological samples, *Biosensors and Bioelectronics*, 2019, 141, 111420.
14. J. Ming, T. Zhu, J. Li, Z. Ye, C. Shi, Z. Guo, J. Wang, X. Chen and N. Zheng, A Novel Cascade Nanoreactor Integrating Two-Dimensional Pd-Ru Nanozyme, Uricase and Red Blood Cell Membrane for Highly Efficient Hyperuricemia Treatment, *Small*, 2021, 17, 2103645.

15. X. P. Liu, Z. J. Zhang, Y. Zhang, Y. J. Guan, Z. Liu, J. S. Ren and X. G. Qu, Artificial Metalloenzyme-Based Enzyme Replacement Therapy for the Treatment of Hyperuricemia, *Advanced Functional Materials*, 2016, 26, 7921-7928.
16. J. Mu, L. Zhang, M. Zhao and Y. Wang, Co3O4 nanoparticles as an efficient catalase mimic: Properties, mechanism and its electrocatalytic sensing application for hydrogen peroxide, *Journal of Molecular Catalysis A: Chemical*, 2013, **378**, 30-37.
17. W. Y. Zhen, Y. Liu, W. Wang, M. C. Zhang, W. X. Hu, X. D. Jia, C. Wang and X. E. Jiang, Specific "Unlocking" of a Nanozyme-Based Butterfly Effect To Break the Evolutionary Fitness of Chaotic Tumors, *Angew Chem Int Edit*, 2020, 59, 9491-9497.
18. M. Gharib, A. Kornowski, H. Noei, W. J. Parak and I. Chakraborty, Protein-Protected Porous Bimetallic AgPt Nanoparticles with pH-Switchable Peroxidase/Catalase-Mimicking Activity, *ACS Materials Letters*, 2019, 1, 310-319.
19. Y. Liu, Y. Qing, L. Jing, W. Zou and R. Guo, Platinum–Copper Bimetallic Colloid Nanoparticle Cluster Nanozymes with Multiple Enzyme-like Activities for Scavenging Reactive Oxygen Species, *Langmuir*, 2021, 37, 7364-7372.
20. K. L. Fan, J. Q. Xi, L. Fan, P. X. Wang, C. H. Zhu, Y. Tang, X. D. Xu, M. M. Liang, B. Jiang, X. Y. Yan and L. Z. Gao, In vivo guiding nitrogen-doped carbon nanozyme for tumor catalytic therapy, *Nature Communications*, 2018, 9, 1440.
21. J. Mu, L. Zhang, M. Zhao and Y. Wang, Catalase Mimic Property of Co3O4 Nanomaterials with Different Morphology and Its Application as a Calcium Sensor, *ACS Applied Materials & Interfaces*, 2014, 6, 7090-7098.
22. J. Fan, J.-J. Yin, B. Ning, X. Wu, Y. Hu, M. Ferrari, G. J. Anderson, J. Wei, Y. Zhao and G. Nie, Direct evidence for catalase and peroxidase activities of ferritin–platinum nanoparticles, *Biomaterials*, 2011, 32, 1611-1618.
23. W. Ma, J. Mao, X. Yang, C. Pan, W. Chen, M. Wang, P. Yu, L. Mao and Y. Li, A single-atom Fe–N4 catalytic site mimicking bifunctional antioxidative enzymes for oxidative stress cytoprotection, *Chemical Communications*, 2019, 55, 159-162.